

ELECTRONIC SUPPLEMENTARY MATERIAL

Vanadium aminophenolates in catechol oxidation: conformity with Finke's common catalyst hypothesis

Pasi Salonen,^a Risto Savela,^b Anssi Peuronen,^a Ari Lehtonen^{a*}

* Corresponding author

^a Group of Inorganic Materials Chemistry, Department of Chemistry, University of Turku, FI-20014 Turku, Finland.

^b Laboratory of Molecular Science and Technology, Åbo Akademi University, FI-20500 Turku, Finland

Contents

GC-FID reference chromatograms	5
GC-MS Chromatograms	8
GC-FID Chromatograms from reactions	10
⁵¹ V NMR spectroscopy	16
Negative mode ESI-MS	18
EPR spectroscopy	30
Identification of complex giving 8-line EPR spectrum	35
Non-catalytic oxidation of 2 to 3	37
References	38

Table of Figures

Figure S 1. All proligands and vanadium complexes used in this study.	1
Figure S 2. The reaction apparatus for 3,5-DTBC oxidation.	3
Figure S 3. Approximate product distribution using column chromatography.	4
Figure S 4. GC-FID chromatogram of authentic 3,5-di-tert-butylcatechol.	5
Figure S 5. GC-FID chromatogram of authentic 3,5-di-tert-butyl-1,2-benzoquinone.	6
Figure S 6. GC-FID chromatogram of authentic 3,5-di-tert-butyl muconic acid anhydride.....	7
Figure S 7. GC-MS chromatogram of 3,5-di-tert-butyl-2-pyrone/ 4,6-di-tert-butyl-2-pyrone.	8
Figure S 8. GC-MS chromatogram of 4,6-di-tert-butyl-2-pyrone/ 3,5-di-tert-butyl-2-pyrone.	8
Figure S 9. GC-MS chromatogram of 4',6,6',8-tetra-tert-butyl-3H-spiro[benzo[b][1,4]dioxine-2,2'-pyran]-3-one.	9
Figure S 10. GC-FID chromatogram from reaction between V1 and 3,5-di-tert-butylcatechol.	10
Figure S 11. GC-FID chromatogram from reaction between V2 and 3,5-di-tert-butylcatechol.	11
Figure S 12. GC-FID chromatogram from reaction between V3 and 3,5-di-tert-butylcatechol.	12
Figure S 13. GC-FID chromatogram from reaction between V4 and 3,5-di-tert-butylcatechol.	13
Figure S 14. GC-FID chromatogram from reaction between V5 and 3,5-di-tert-butylcatechol.	14
Figure S 15. GC-FID chromatogram from reaction between V6 and 3,5-di-tert-butylcatechol.	15
Figure S 16. Full width ⁵¹ V NMR 48-hour post-reaction spectra of V1–V6 in CDCl ₃ after treatment with 100 eq. 3,5-DTBC. Very faint ⁵¹ V NMR signals can be seen at ca. +1550 ppm vs. VOCl ₃ in the case of V3 and V4 (highlighted in red).....	16
Figure S 17. Full width ⁵¹ V NMR spectra of V1–V6 in CDCl ₃ immediately after treatment with 100 eq. 3,5-DTBC.	17
Figure S 18. Negative mode ESI-MS spectrum of V1 + 100 eq. 3,5-DTBC at reaction t = 30 min.	18
Figure S 19. Negative mode post-reaction ESI-MS spectrum of V1 + 100 eq. 3,5-DTBC at reaction t = 48 h.	19
Figure S 20. Negative mode ESI-MS spectrum of V1 + 100 eq. 3,5-DTBC at reaction t = 30 min.	20
Figure S 21. Negative mode post-reaction ESI-MS spectrum of V2 + 100 eq. 3,5-DTBC at reaction t = 48 h.	21
Figure S 22. Negative mode ESI-MS spectrum of V3 + 100 eq. 3,5-DTBC at reaction t = 30 min.	22
Figure S 23. Negative mode post-reaction ESI-MS spectrum of V3 + 100 eq. 3,5-DTBC at reaction t = 48 h.	23
Figure S 24. Negative mode ESI-MS spectrum of V4 + 100 eq. 3,5-DTBC at reaction t = 30 min.	24
Figure S 25. Negative mode post-reaction ESI-MS spectrum of V4 + 100 eq. 3,5-DTBC at reaction t = 48 h.	25
Figure S 26. Negative mode ESI-MS spectrum of V5 + 100 eq. 3,5-DTBC at reaction t = 30 min.	26
Figure S 27. Negative mode post-reaction ESI-MS spectrum of V5 + 100 eq. 3,5-DTBC at reaction t = 48 h.	27
Figure S 28. Negative mode ESI-MS spectrum of V6 + 100 eq. 3,5-DTBC at reaction t = 30 min.	28
Figure S 29. Negative mode post-reaction ESI-MS spectrum of V6 + 100 eq. 3,5-DTBC at reaction t = 48 h.	29
Figure S 30. Ambient atmosphere center field EPR spectra of V1–V6 in toluene recorded at RT 30 min after treatment with 100 eq. 3,5-DTBC.....	31

Figure S 31. Ambient atmosphere center field EPR spectra of V1–V6 in toluene recorded at RT 6 hours after treatment with 100 eq. 3,5-DTBC.....	32
Figure S 32. Ambient atmosphere center field EPR spectra of V1–V6 in toluene recorded at RT 24 hours after treatment with 100 eq. 3,5-DTBC.....	33
Figure S 33. Ambient atmosphere center field EPR spectra of V1–V6 in toluene recorded at RT 72 hours after treatment with 100 eq. 3,5-DTBC.....	34
Figure S 34. Newly recorded ambient atmosphere center field EPR spectrum of V2 in toluene at RT 48 hours after treatment with 100 eq. 3,5-DTBC.....	35
Figure S 35. Negative mode ESI-MS spectrum of V2 at 48 hours after treatment with 100 eq. 3,5-DTBC.	36

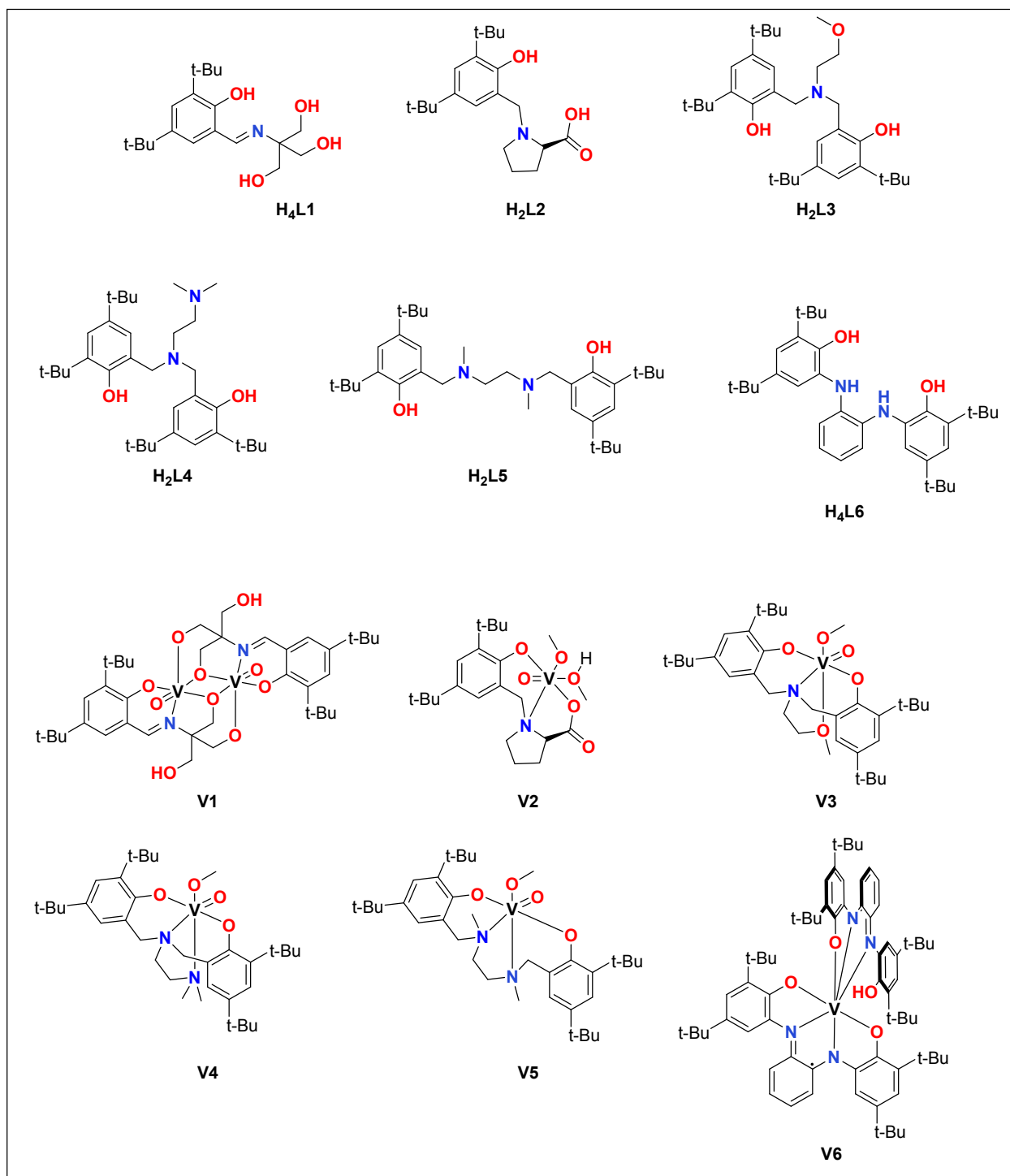
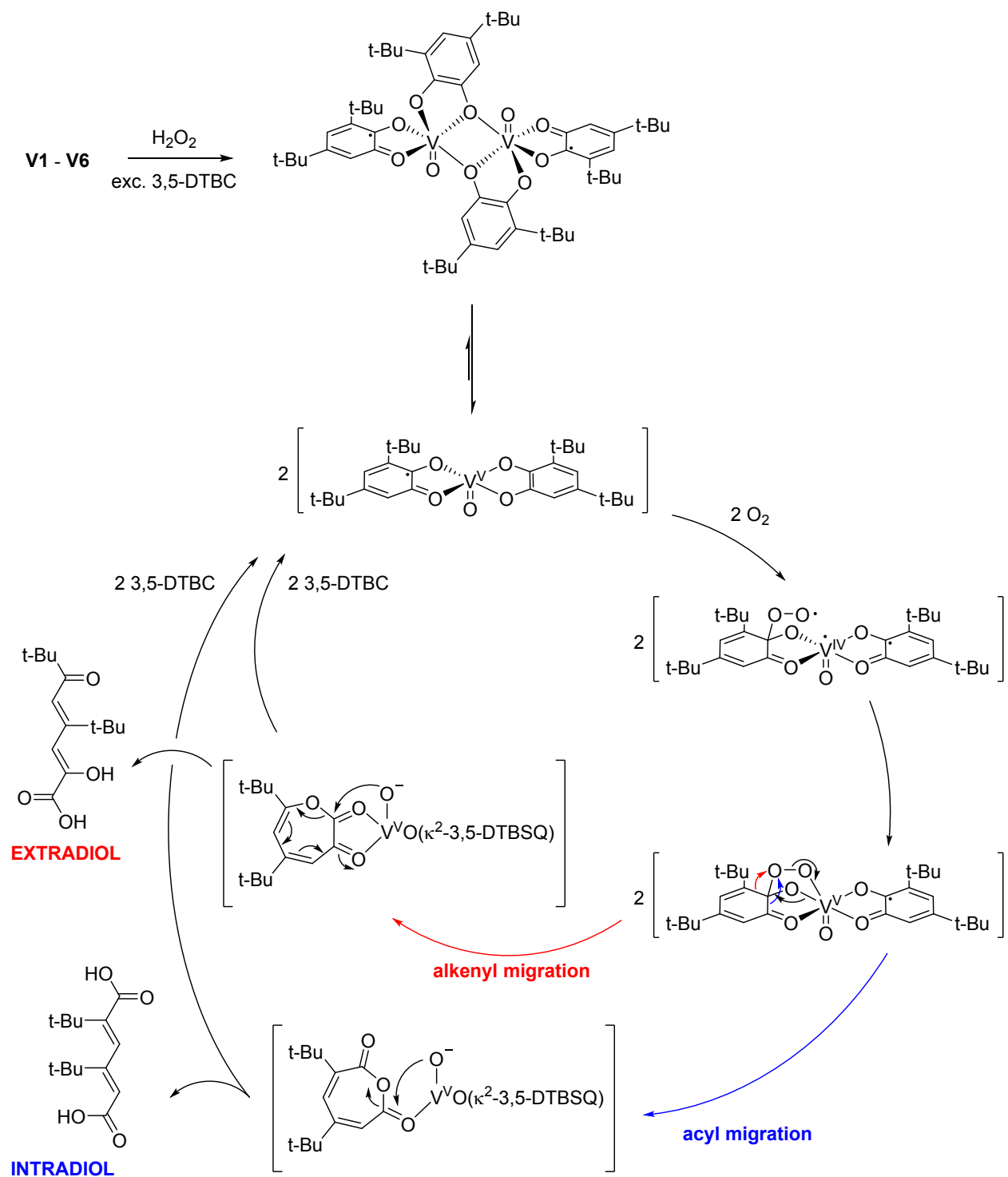


Figure S 1. All proligands and vanadium complexes used in this study.



Scheme S 1. The overall mechanism of vanadium-catalyzed intra- and extradiol catechol dioxygenase reactions as proposed by Finke. **V1–V6** have been fitted to the mechanism.[1]

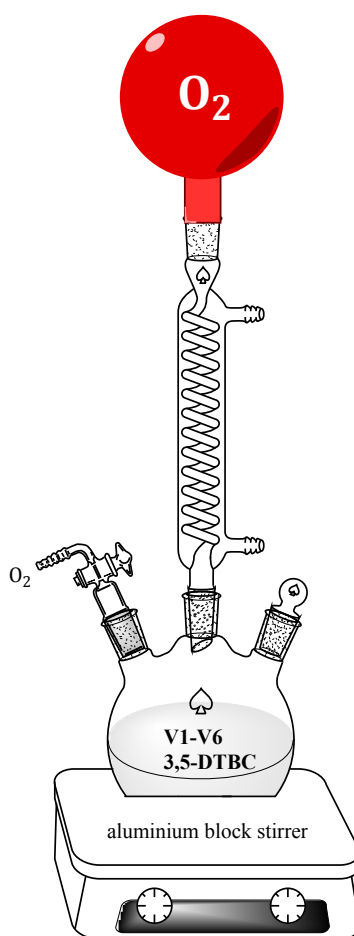


Figure S 2. The reaction apparatus for 3,5-DTBC oxidation.

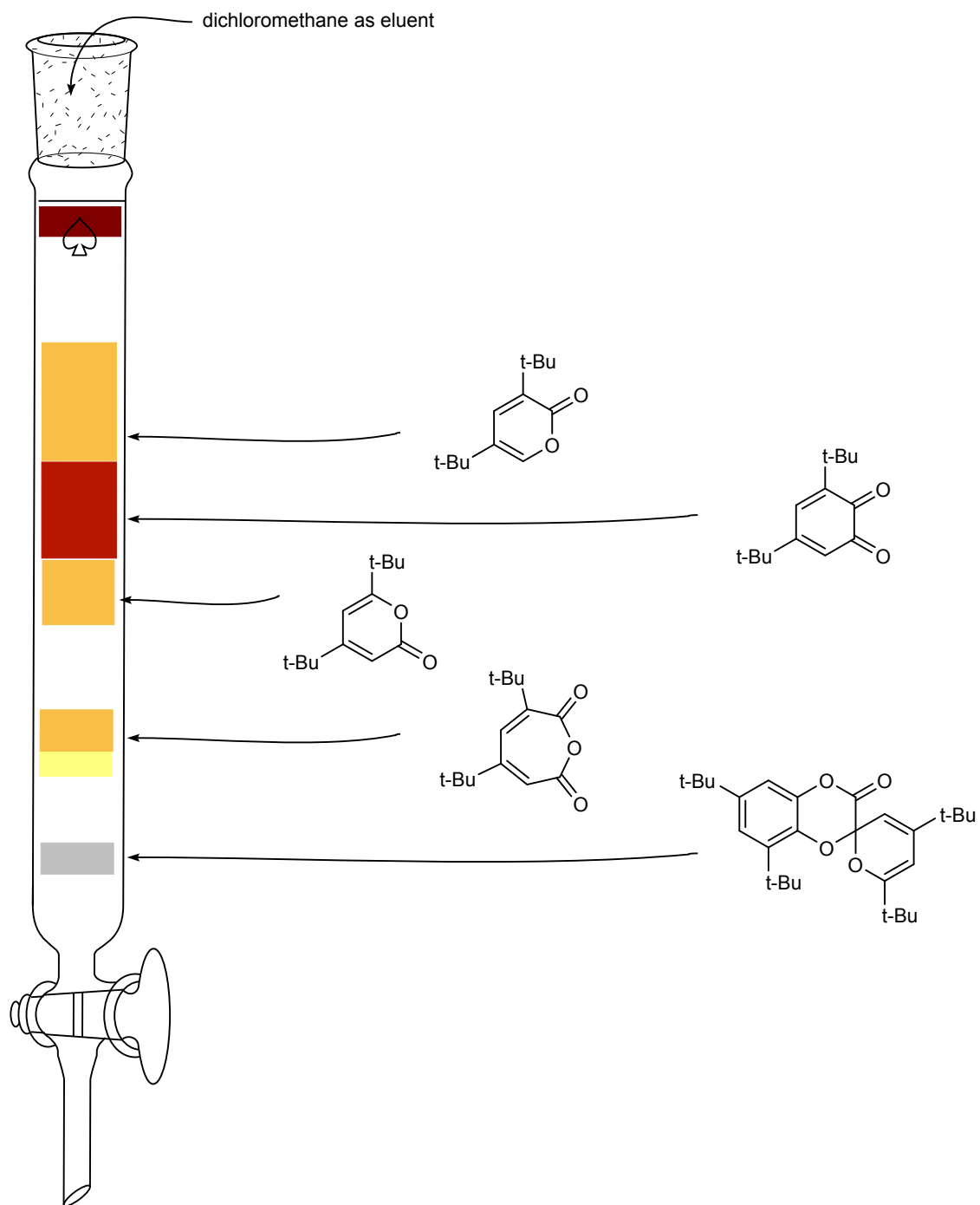


Figure S 3. Approximate product distribution using column chromatography.

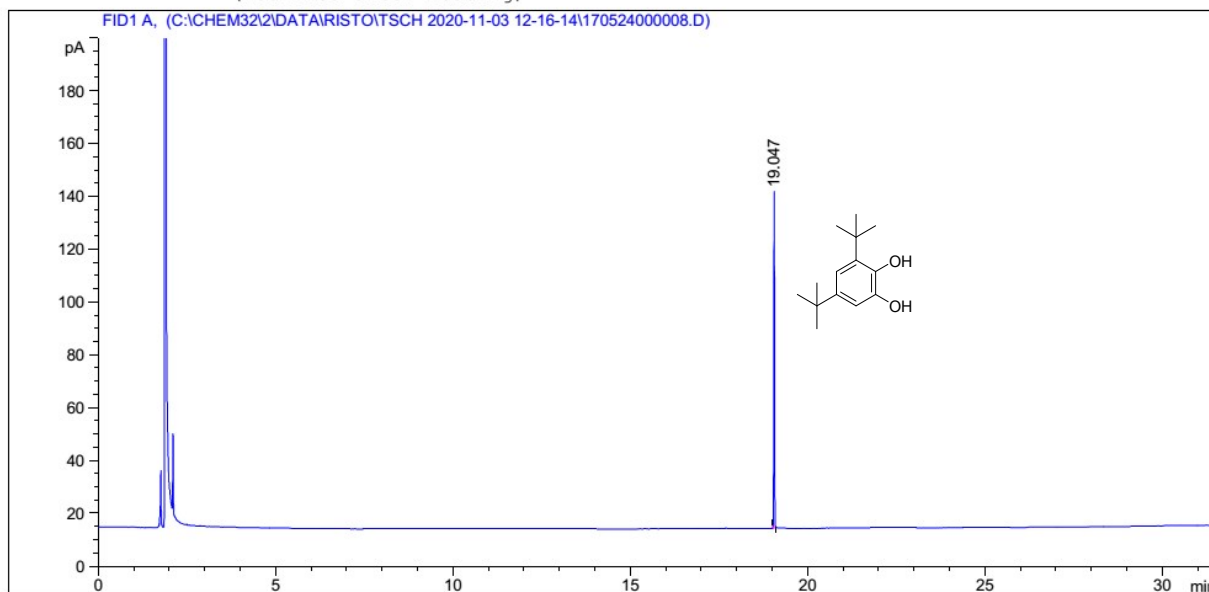
GC-FID reference chromatograms

Data File C:\CHEM32\2\DATA\RISTO\TSCH 2020-11-03 12-16-14\170524000008.D

Sample Name: 3,5-ditbutcat

```
=====
Acq. Operator   : RMS                               Seq. Line :    7
Acq. Instrument : Instrument 2                       Location  : Vial 7
Injection Date  : 03-Nov-20, 16:54:07              Inj       :    1
                                                    Inj Volume: 1 µl

Acq. Method     : C:\CHEM32\2\DATA\RISTO\TSCH 2020-11-03 12-16-14\AA-DEFAULT.M
Last changed    : 9/11/2020 12:47:18 PM by RMS
Analysis Method : C:\CHEM32\2\METHODS\RMS1_HP1.M
Last changed    : 11/5/2020 11:37:10 AM by RMS
                (modified after loading)
=====
```



Signal 1: FID1 A,

Peak #	RetTime [min]	Type	Width [min]	Area [pA*s]	Height [pA]	Area %
1	19.047	BB	0.0236	191.71303	127.17262	1.000e2

Totals : 191.71303 127.17262

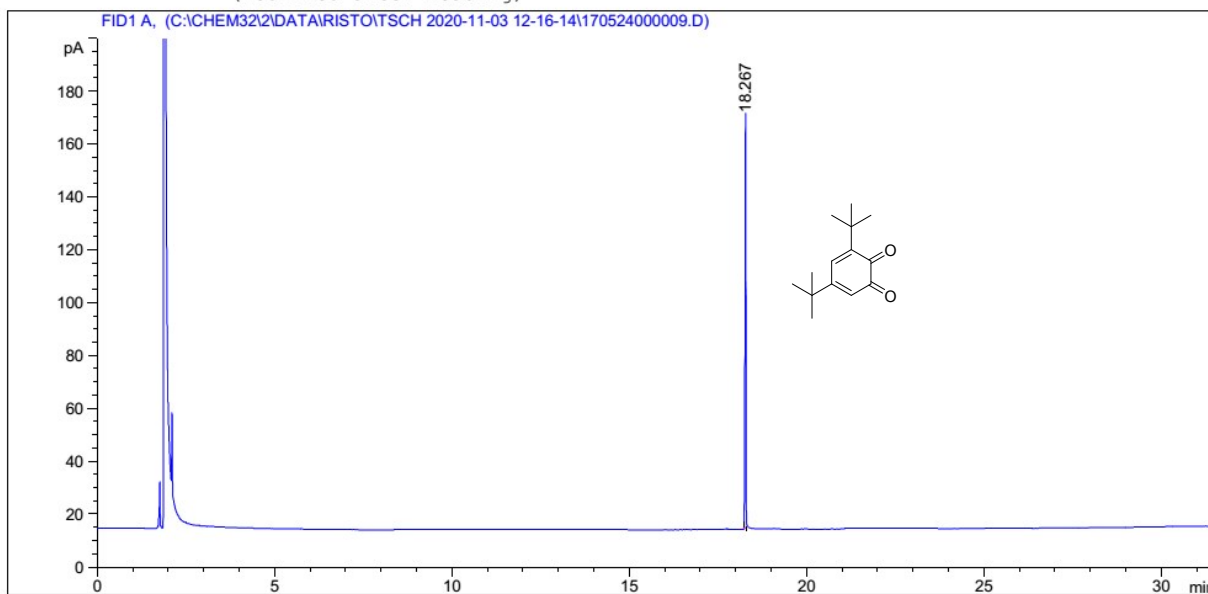
Figure S 4. GC-FID chromatogram of authentic 3,5-di-tert-butylcatechol.

Data File C:\CHEM32\2\DATA\RISTO\TSCHE 2020-11-03 12-16-14\170524000009.D

Sample Name: 3,5-ditbuqin

```
=====
Acq. Operator   : RMS                               Seq. Line :    8
Acq. Instrument : Instrument 2                       Location  : Vial 8
Injection Date  : 03-Nov-20, 17:33:41              Inj       :    1
                                                    Inj Volume: 1 µl

Acq. Method     : C:\CHEM32\2\DATA\RISTO\TSCHE 2020-11-03 12-16-14\AA-DEFAULT.M
Last changed    : 9/11/2020 12:47:18 PM by RMS
Analysis Method : C:\CHEM32\2\METHODS\RMS1_HP1.M
Last changed    : 11/5/2020 11:37:10 AM by RMS
                (modified after loading)
=====
```



Signal 1: FID1 A,

Peak #	RetTime [min]	Type	Width [min]	Area [pA*s]	Height [pA]	Area %
1	18.267	BB	0.0268	264.38159	155.59264	1.000e2

Totals : 264.38159 155.59264

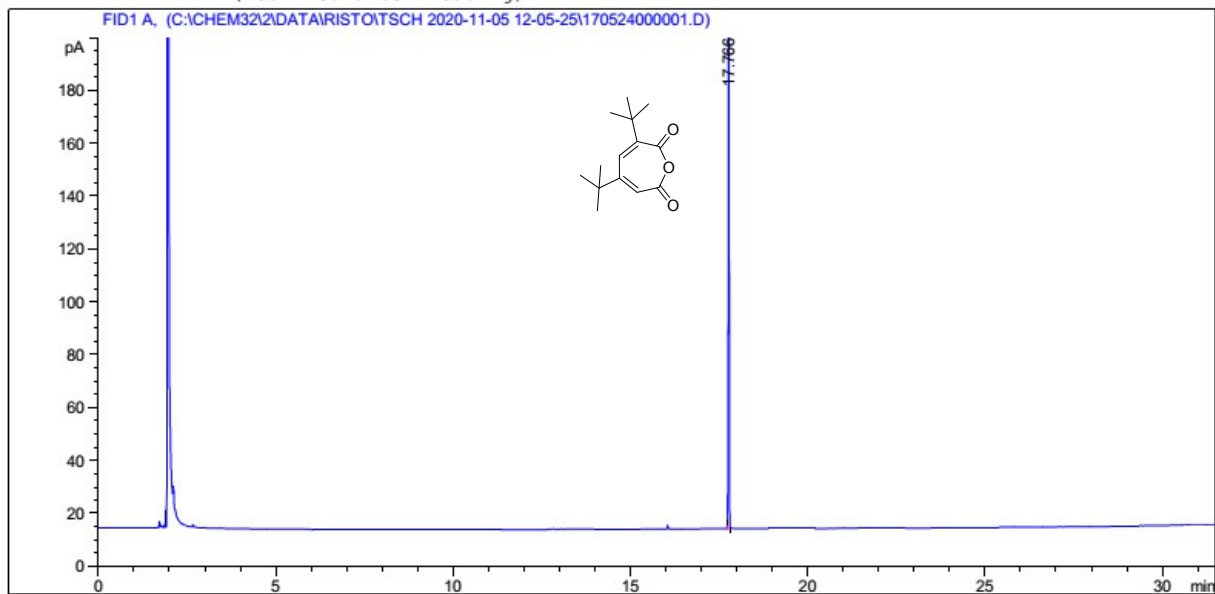
Figure S 5. GC-FID chromatogram of authentic 3,5-di-tert-butyl-1,2-benzoquinone.

Data File C:\CHEM32\2\DATA\RISTO\TSCH 2020-11-05 12-05-25\170524000001.D
Sample Name: 3,5-DitbuAnhydr

=====

Acq. Operator	: RMS	Seq. Line	: 1
Acq. Instrument	: Instrument 2	Location	: Vial 1
Injection Date	: 05-Nov-20, 12:06:44	Inj	: 1
		Inj Volume	: 1 µl

Acq. Method : C:\CHEM32\2\DATA\RISTO\TSCH 2020-11-05 12-05-25\AA-DEFAULT.M
Last changed : 9/11/2020 12:47:18 PM by RMS
Analysis Method : C:\CHEM32\2\METHODS\RMS1_HP1.M
Last changed : 11/5/2020 1:01:05 PM by RMS
(modified after loading)



Signal 1: FID1 A,

Peak #	RetTime [min]	Type	Width [min]	Area [pA*s]	Height [pA]	Area %
1	17.766	BB	0.0253	325.28619	196.35132	1.000e2

Totals : 325.28619 196.35132

Figure S 6. GC-FID chromatogram of authentic 3,5-di-tert-butyl muconic acid anhydride.

GC-MS Chromatograms

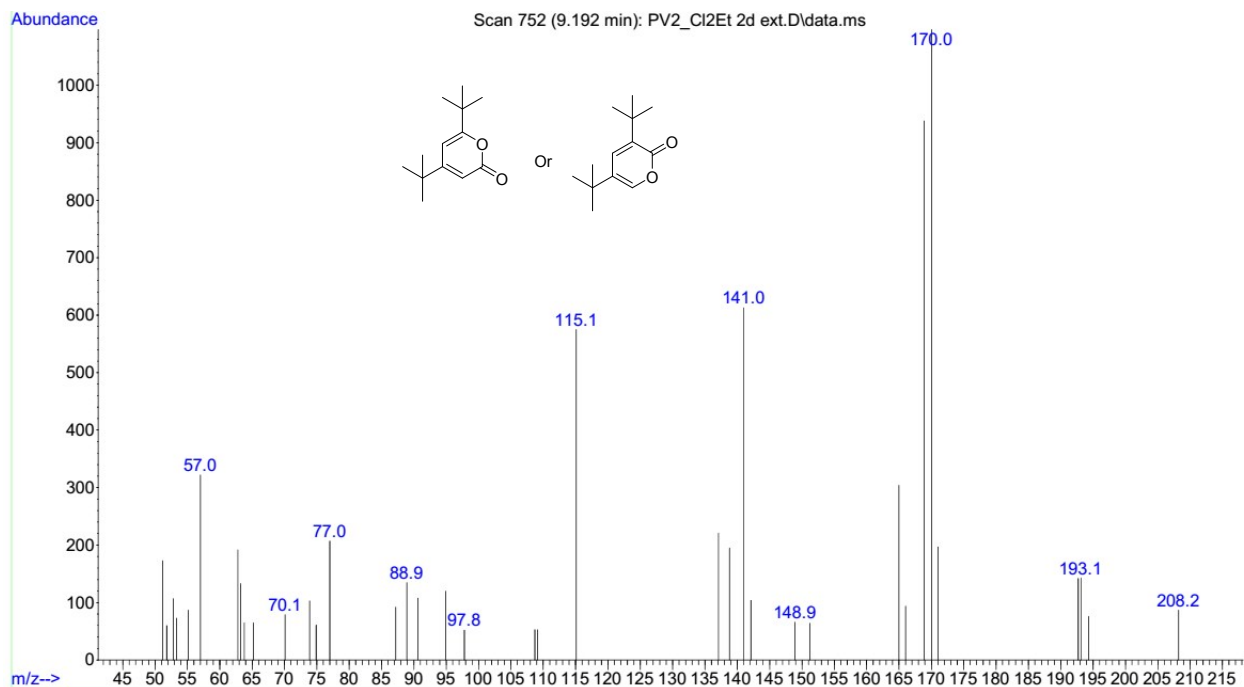


Figure S 7. GC-MS chromatogram of 3,5-di-tert-butyl-2-pyrone/ 4,6-di-tert-butyl-2-pyrone.

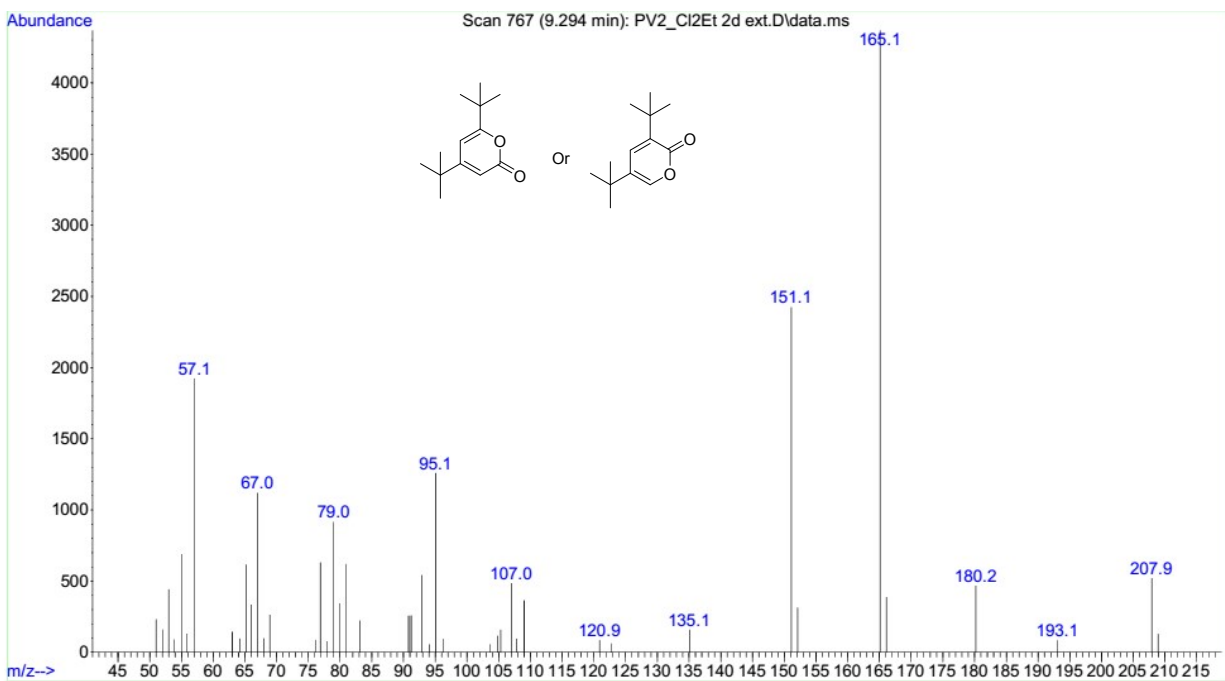


Figure S 8. GC-MS chromatogram of 4,6-di-tert-butyl-2-pyrone/ 3,5-di-tert-butyl-2-pyrone.

GC-FID Chromatograms from reactions

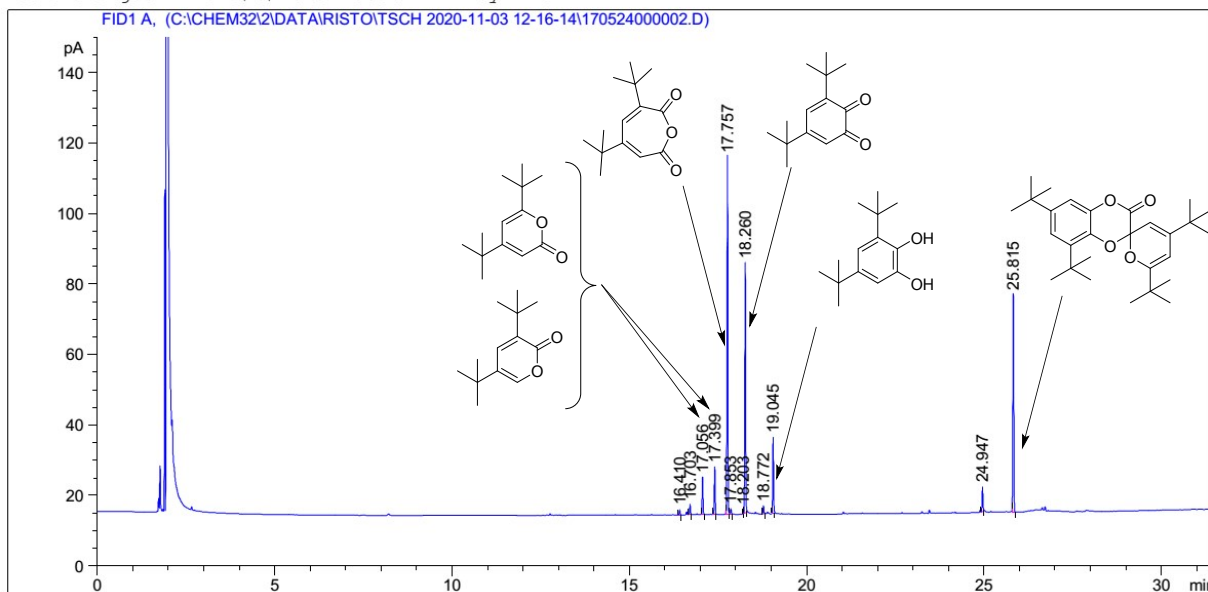
Data File C:\CHEM32\2\DATA\RISTO\TSCH 2020-11-03 12-16-14\170524000002.D

Sample Name: PV1

```

=====
Acq. Operator   : RMS                               Seq. Line :    1
Acq. Instrument : Instrument 2                       Location  : Vial 1
Injection Date  : 03-Nov-20, 12:57:09              Inj       :    2
                                                    Inj Volume: 1 µl

Acq. Method    : C:\CHEM32\2\DATA\RISTO\TSCH 2020-11-03 12-16-14\AA-DEFAULT.M
Last changed   : 9/11/2020 12:47:18 PM by RMS
Analysis Method : C:\CHEM32\2\METHODS\RMS1_HP1.M
Last changed   : 3/6/2019 7:50:44 AM by RMS
    
```



Signal 1: FID1 A,

Peak #	RetTime [min]	Type	Width [min]	Area [pA*s]	Height [pA]	Area %
7	18.203	BV	0.0223	1.81505	1.29941	0.37243
8	18.260	VB	0.0260	115.38091	70.78101	23.67478
9	18.772	BB	0.0253	3.83337	2.32233	0.78656
1	16.410	BB	0.0251	2.35078	1.43703	0.48235
2	16.703	BB	0.0256	4.66719	2.93486	0.95765
3	17.056	BB	0.0258	17.06114	10.59470	3.50074
4	17.399	BB	0.0258	21.80996	13.50355	4.47514
5	17.757	BB	0.0261	166.28056	101.34944	34.11878
6	17.853	BB	0.0280	2.91353	1.54254	0.59782
Totals :				487.35782	296.07992	

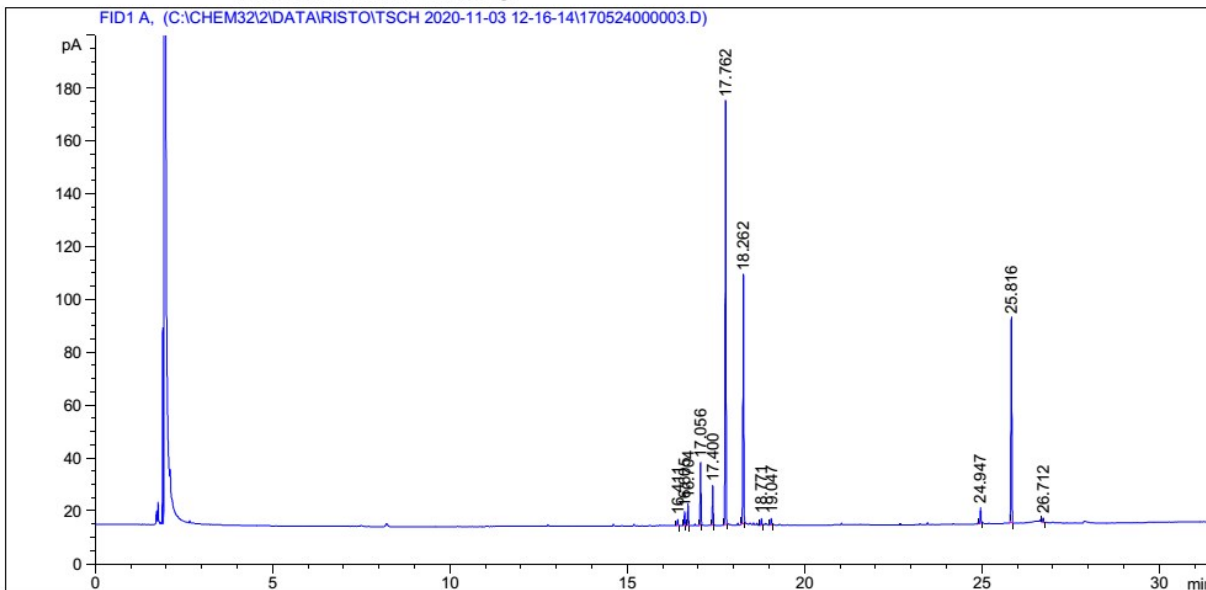
Figure S 10. GC-FID chromatogram from reaction between V1 and 3,5-di-tert-butylcatechol.

Data File C:\CHEM32\2\DATA\RISTO\TSCH 2020-11-03 12-16-14\170524000003.D
 Sample Name: PV2

```

=====
Acq. Operator   : RMS                               Seq. Line :    2
Acq. Instrument : Instrument 2                     Location  : Vial 2
Injection Date  : 03-Nov-20, 13:36:48             Inj       :    1
                                                    Inj Volume: 1 µl

Acq. Method     : C:\CHEM32\2\DATA\RISTO\TSCH 2020-11-03 12-16-14\AA-DEFAULT.M
Last changed    : 9/11/2020 12:47:18 PM by RMS
Analysis Method : C:\CHEM32\2\METHODS\RMS1_HP1.M
Last changed    : 11/5/2020 11:37:10 AM by RMS
                  (modified after loading)
  
```



Peak #	RetTime [min]	Type	Width [min]	Area [pA*s]	Height [pA]	Area %
6	17.762	BB	0.0260	260.71616	159.82800	39.73150
7	18.262	BB	0.0258	152.05272	94.10952	23.17188
8	18.771	BB	0.0255	4.01216	2.53527	0.61143
9	19.047	BB	0.0270	4.53595	2.52044	0.69125
10	24.947	BB	0.0246	9.47045	5.94118	1.44324
11	25.816	BB	0.0272	133.51425	77.29706	20.34673
12	26.712	BB	0.0268	2.70974	1.59980	0.41295
Totals :				656.19515	399.05023	

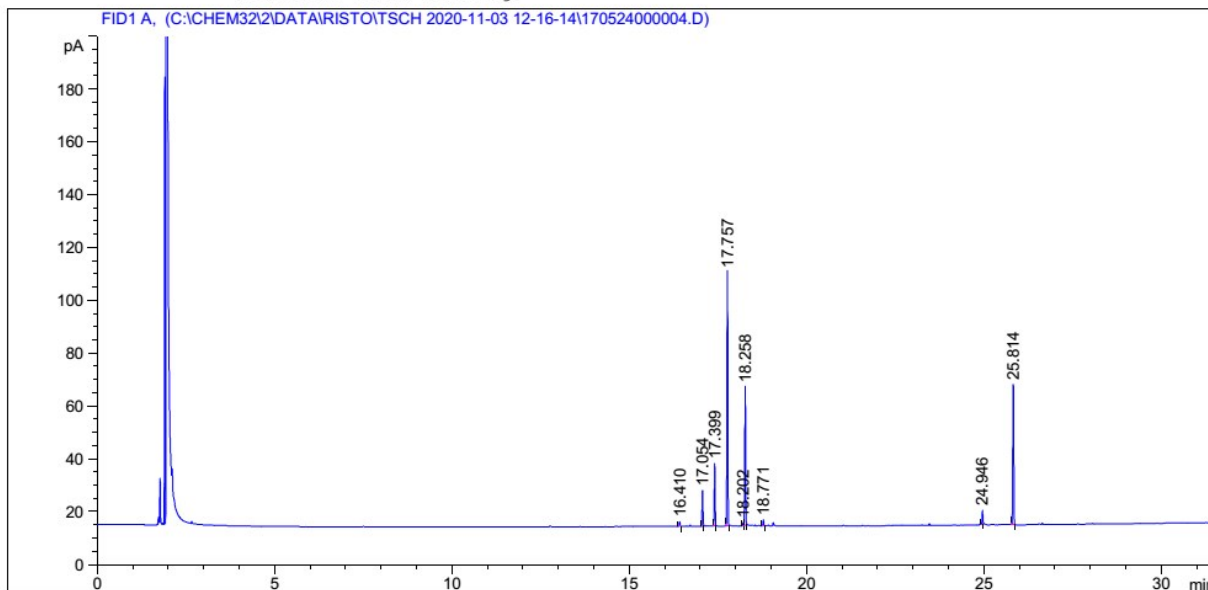
Figure S 11. GC-FID chromatogram from reaction between V2 and 3,5-di-tert-butylcatechol.

Data File C:\CHEM32\2\DATA\RISTO\TSCH 2020-11-03 12-16-14\170524000004.D
 Sample Name: PV3

```

=====
Acq. Operator   : RMS                               Seq. Line :    3
Acq. Instrument : Instrument 2                       Location  : Vial 3
Injection Date  : 03-Nov-20, 14:16:10                Inj       :    1
                                                    Inj Volume: 1 µl

Acq. Method     : C:\CHEM32\2\DATA\RISTO\TSCH 2020-11-03 12-16-14\AA-DEFAULT.M
Last changed    : 9/11/2020 12:47:18 PM by RMS
Analysis Method : C:\CHEM32\2\METHODS\RMS1_HPL.M
Last changed    : 11/5/2020 11:37:10 AM by RMS
                  (modified after loading)
  
```



Signal 1: FID1 A,

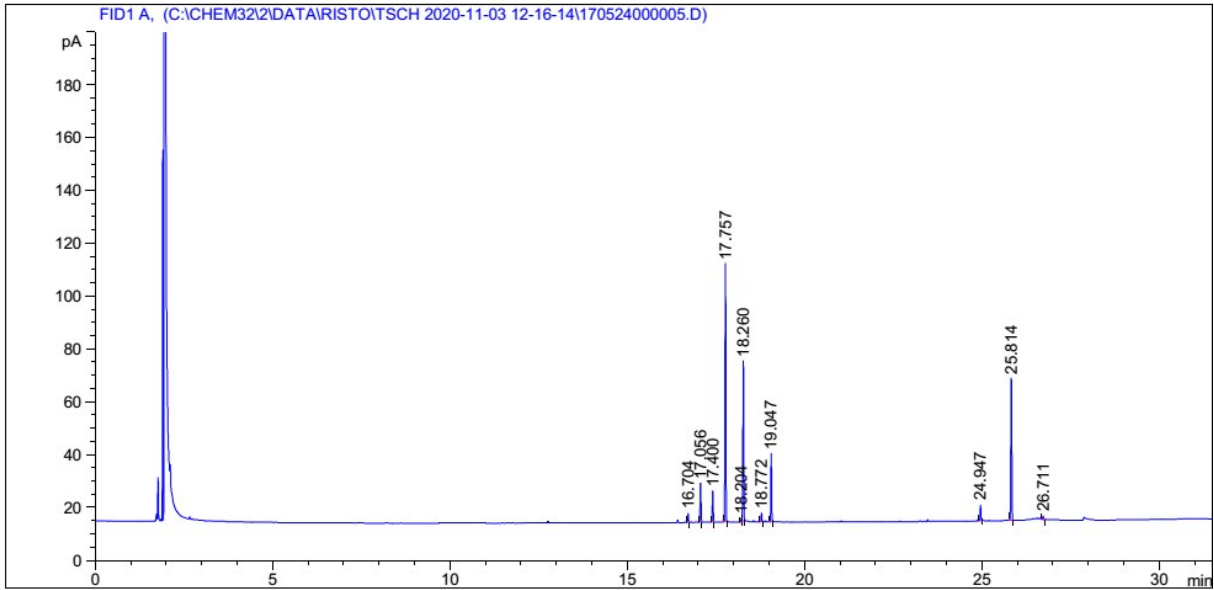
Peak #	RetTime [min]	Type	Width [min]	Area [pA*s]	Height [pA]	Area %	Peak #	RetTime [min]	Type	Width [min]	Area [pA*s]	Height [pA]	Area %
1	16.410	BB	0.0253	3.11322	1.88092	0.76735	6	18.258	VB	0.0244	82.69583	52.29529	20.38286
2	17.054	BB	0.0260	21.98598	13.48777	5.41910	7	18.771	BB	0.0259	3.75358	2.31957	0.92518
3	17.399	BB	0.0256	37.67933	23.66763	9.28720	8	24.946	BB	0.0247	8.50840	5.30906	2.09715
4	17.757	BB	0.0258	154.80180	96.05413	38.15554	9	25.814	BB	0.0271	91.44478	53.07932	22.53930
5	18.202	BV	0.0237	1.72961	1.20902	0.42632	Totals :				405.71255	249.30270	

Figure S 12. GC-FID chromatogram from reaction between V3 and 3,5-di-tert-butylcatechol.

Data File C:\CHEM32\2\DATA\RISTO\TSCH 2020-11-03 12-16-14\170524000005.D
 Sample Name: PV4

```
=====
Acq. Operator   : RMS                               Seq. Line :    4
Acq. Instrument : Instrument 2                       Location  : Vial 4
Injection Date  : 03-Nov-20, 14:55:44              Inj       :    1
                                                    Inj Volume: 1 µl

Acq. Method     : C:\CHEM32\2\DATA\RISTO\TSCH 2020-11-03 12-16-14\AA-DEFAULT.M
Last changed    : 9/11/2020 12:47:18 PM by RMS
Analysis Method : C:\CHEM32\2\METHODS\RMS1_HP1.M
Last changed    : 11/5/2020 11:37:10 AM by RMS
                (modified after loading)
=====
```



Signal 1: FID1 A,

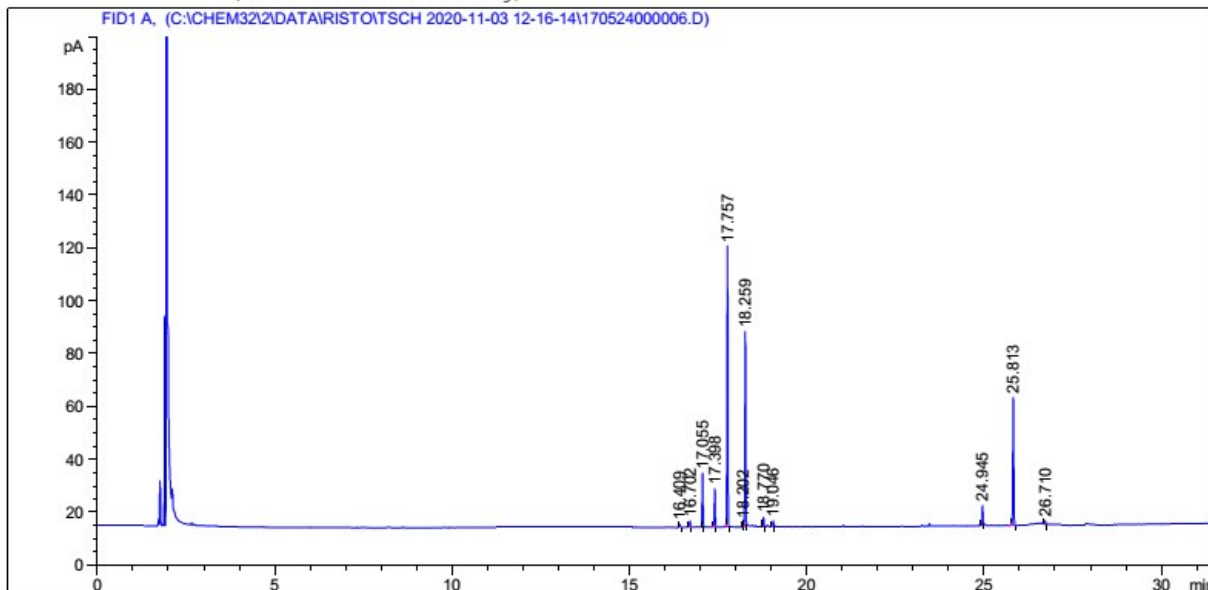
Peak #	RetTime [min]	Type	Width [min]	Area [pA*s]	Height [pA]	Area %
6	18.260	VB	0.0246	96.76943	60.66752	21.43655
7	18.772	BB	0.0261	5.55104	3.38427	1.22968
8	19.047	BB	0.0236	38.78708	25.65917	8.59219
9	24.947	BB	0.0263	9.56491	5.79613	2.11884
10	25.814	BB	0.0274	93.98115	53.67443	20.81888
11	26.711	BB	0.0263	2.21271	1.33684	0.49016
Totals :				451.42266	279.47980	

Figure S 13. GC-FID chromatogram from reaction between **V4** and 3,5-di-tert-butylcatechol.

Data File C:\CHEM32\2\DATA\RISTO\TSCH 2020-11-03 12-16-14\170524000006.D
 Sample Name: PV5

```
=====
Acq. Operator   : RMS                               Seq. Line :    5
Acq. Instrument : Instrument 2                     Location  : Vial 5
Injection Date  : 03-Nov-20, 15:35:06             Inj       :    1
                                                    Inj Volume: 1 µl

Acq. Method    : C:\CHEM32\2\DATA\RISTO\TSCH 2020-11-03 12-16-14\AA-DEFAULT.M
Last changed   : 9/11/2020 12:47:18 PM by RMS
Analysis Method : C:\CHEM32\2\METHODS\RMS1_HPL.M
Last changed   : 11/5/2020 11:37:10 AM by RMS
                (modified after loading)
=====
```



Peak #	RetTime [min]	Type	Width [min]	Area [pA*s]	Height [pA]	Area %
6	18.202	BV	0.0238	2.02898	1.41171	0.44007
7	18.259	VB	0.0245	116.34693	73.24644	25.23467
8	18.770	BB	0.0259	5.77262	3.57059	1.25203
9	19.046	BB	0.0276	3.99142	2.15456	0.86571
1	16.409	BB	0.0249	2.03157	1.25662	0.44063
2	16.702	BB	0.0257	3.94417	2.45958	0.85546
3	17.055	BB	0.0246	32.23523	20.18182	6.99155
4	17.398	BB	0.0259	23.45242	14.44827	5.08663
5	17.757	BB	0.0248	170.05820	105.74660	36.88419
Totals :				461.05990	281.67159	

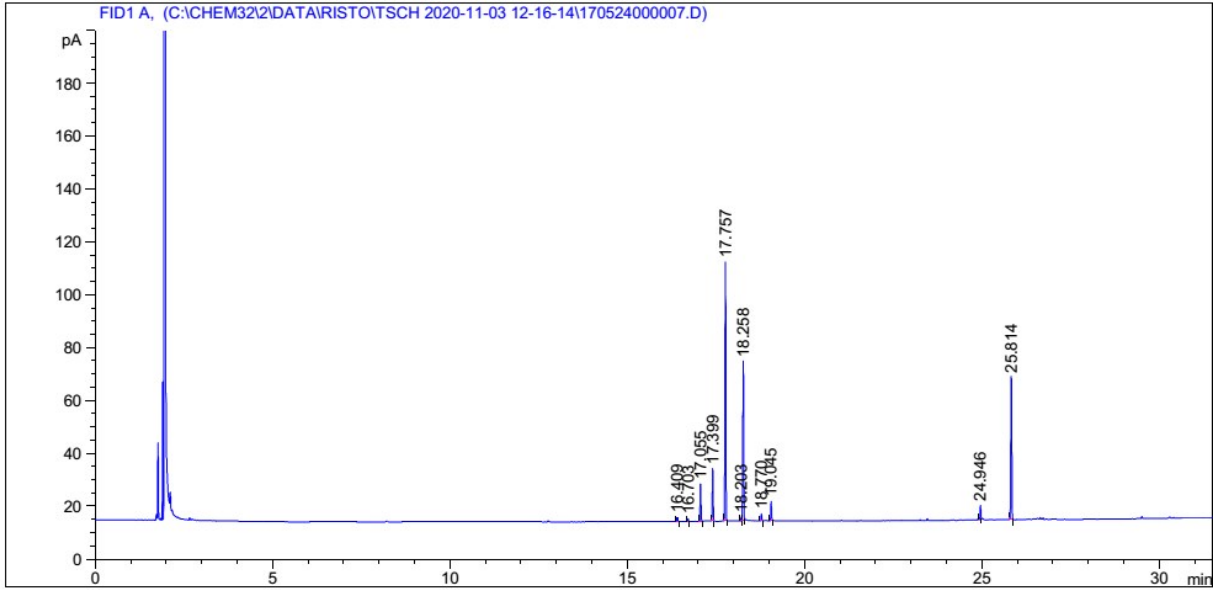
Figure S 14. GC-FID chromatogram from reaction between V5 and 3,5-di-tert-butylcatechol.

Data File C:\CHEM32\2\DATA\RISTO\TSCH 2020-11-03 12-16-14\170524000007.D
 Sample Name: PV6

```

=====
Acq. Operator   : RMS                               Seq. Line :    6
Acq. Instrument : Instrument 2                       Location  : Vial 6
Injection Date  : 03-Nov-20, 16:14:41              Inj       :    1
                                                    Inj Volume: 1 µl

Acq. Method    : C:\CHEM32\2\DATA\RISTO\TSCH 2020-11-03 12-16-14\AA-DEFAULT.M
Last changed   : 9/11/2020 12:47:18 PM by RMS
Analysis Method: C:\CHEM32\2\METHODS\RMS1_HPL.M
Last changed   : 11/5/2020 11:37:10 AM by RMS
                (modified after loading)
  
```



Peak #	RetTime [min]	Type	Width [min]	Area [pA*s]	Height [pA]	Area %
6	18.203	BV	0.0227	2.10987	1.47100	0.48406
7	18.258	VB	0.0258	96.88969	60.24203	22.22906
8	18.770	BB	0.0245	4.22168	2.65918	0.96856
9	19.045	BB	0.0257	11.62446	7.26762	2.66696
10	24.946	BB	0.0246	8.58679	5.37223	1.97004
11	25.814	BB	0.0278	95.88039	53.87613	21.99750
Totals :				435.86957	265.70329	

Peak #	RetTime [min]	Type	Width [min]	Area [pA*s]	Height [pA]	Area %
1	16.409	BB	0.0249	2.70273	1.67173	0.62008
2	16.703	BB	0.0247	1.86127	1.16032	0.42702
3	17.055	BB	0.0256	22.41176	14.04570	5.14185
4	17.399	BB	0.0246	31.84826	19.94337	7.30683
5	17.757	BB	0.0258	157.73267	97.99398	36.18804

Figure S 15. GC-FID chromatogram from reaction between V6 and 3,5-di-tert-butylcatechol.

^{51}V NMR spectroscopy

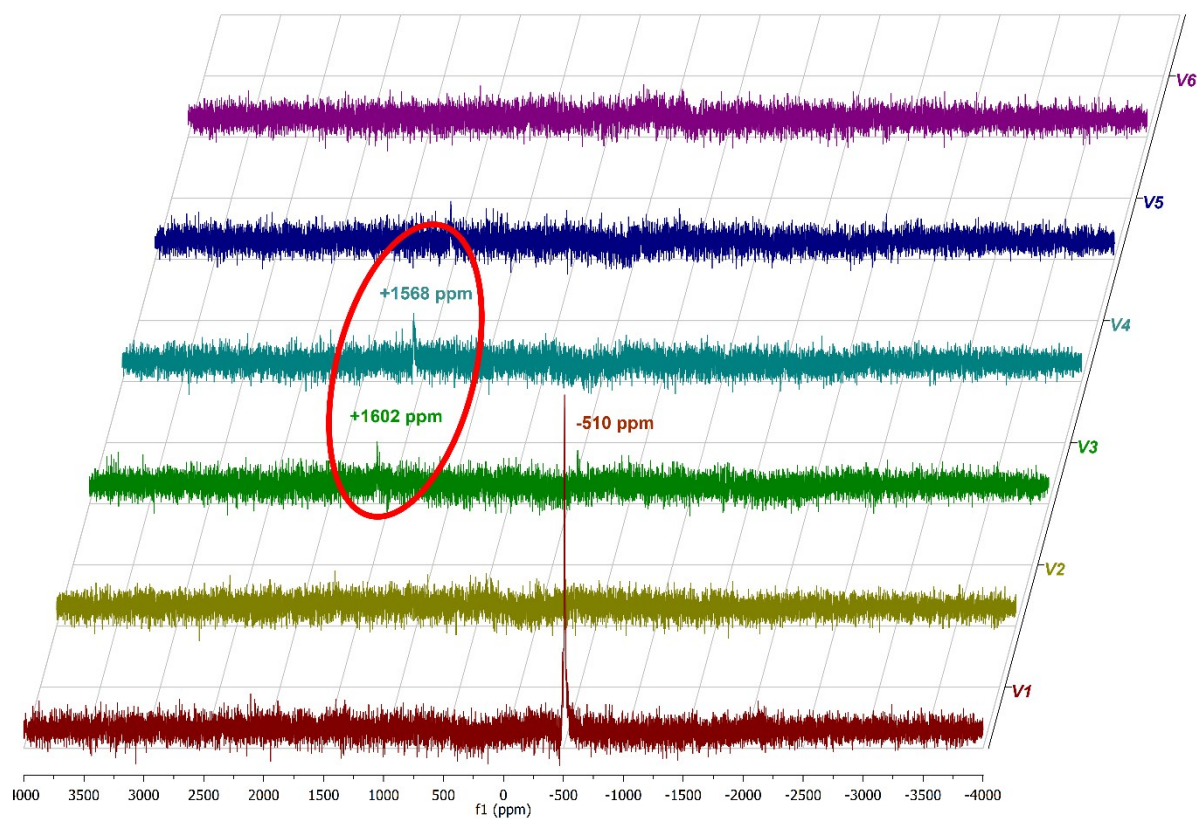


Figure S 16. Full width ^{51}V NMR 48-hour post-reaction spectra of **V1–V6** in CDCl_3 after treatment with 100 eq. 3,5-DTBC. Very faint ^{51}V NMR signals can be seen at ca. +1550 ppm vs. VOCl_3 in the case of **V3** and **V4** (highlighted in red).

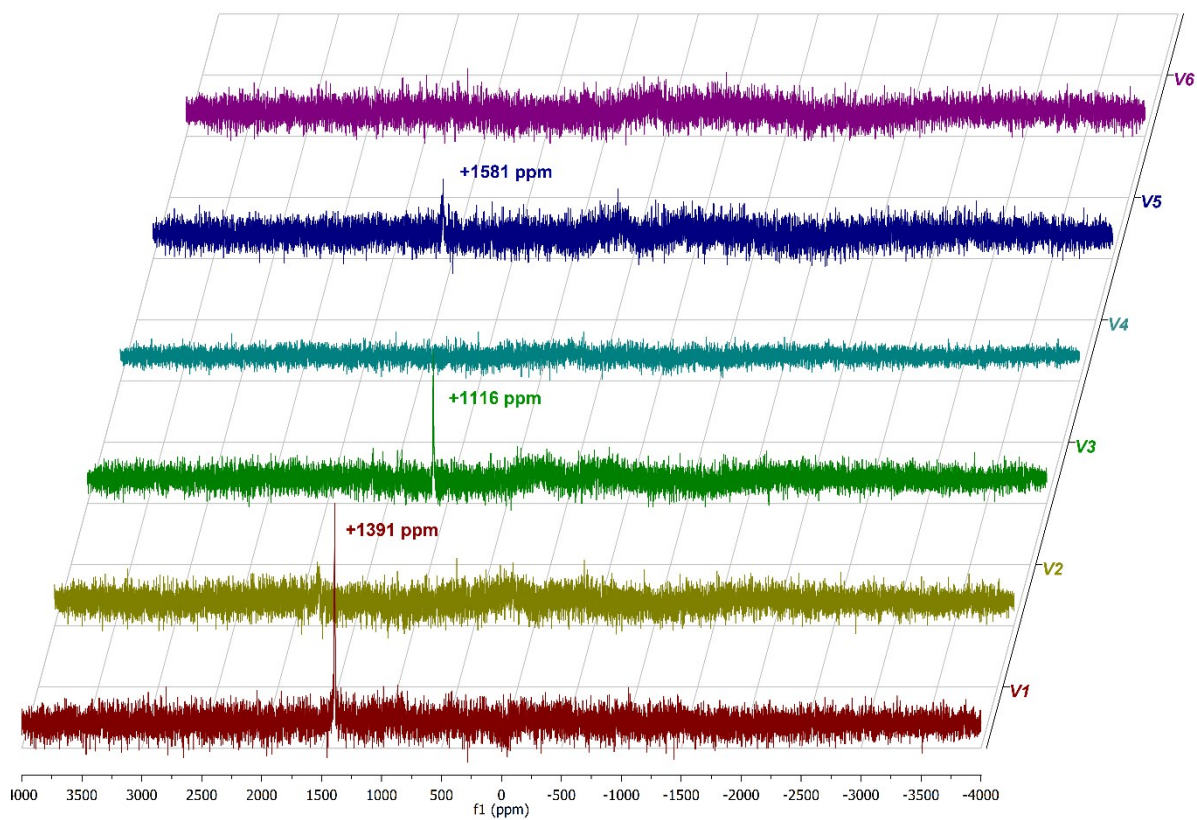


Figure S 17. Full width ^{51}V NMR spectra of **V1–V6** in CDCl_3 immediately after treatment with 100 eq. 3,5-DTBC.

Negative mode ESI-MS

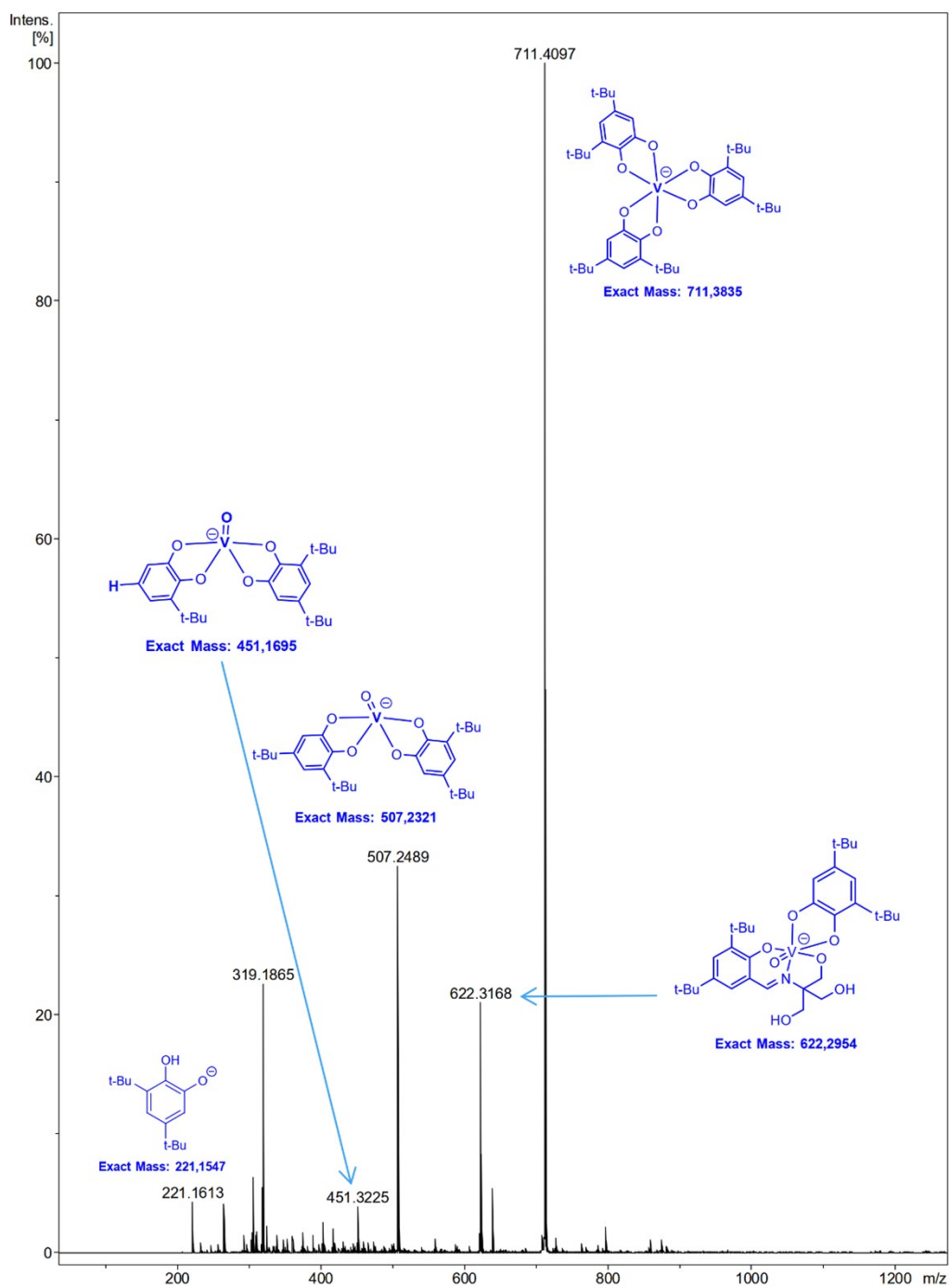


Figure S 18. Negative mode ESI-MS spectrum of **V1** + 100 eq. 3,5-DTBC at reaction $t = 30$ min.

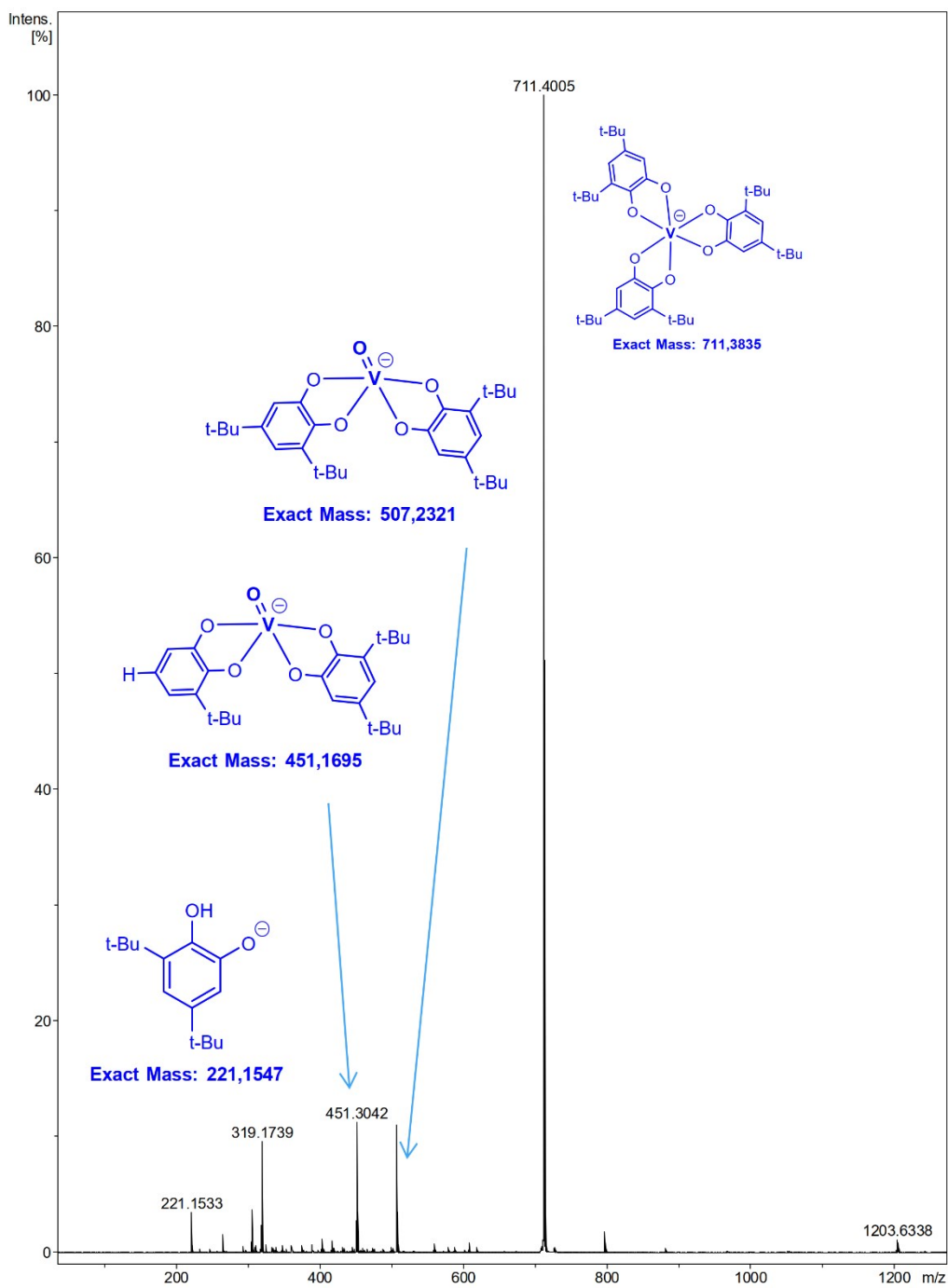


Figure S 20. Negative mode ESI-MS spectrum of **V1** + 100 eq. 3,5-DTBC at reaction $t = 30$ min.

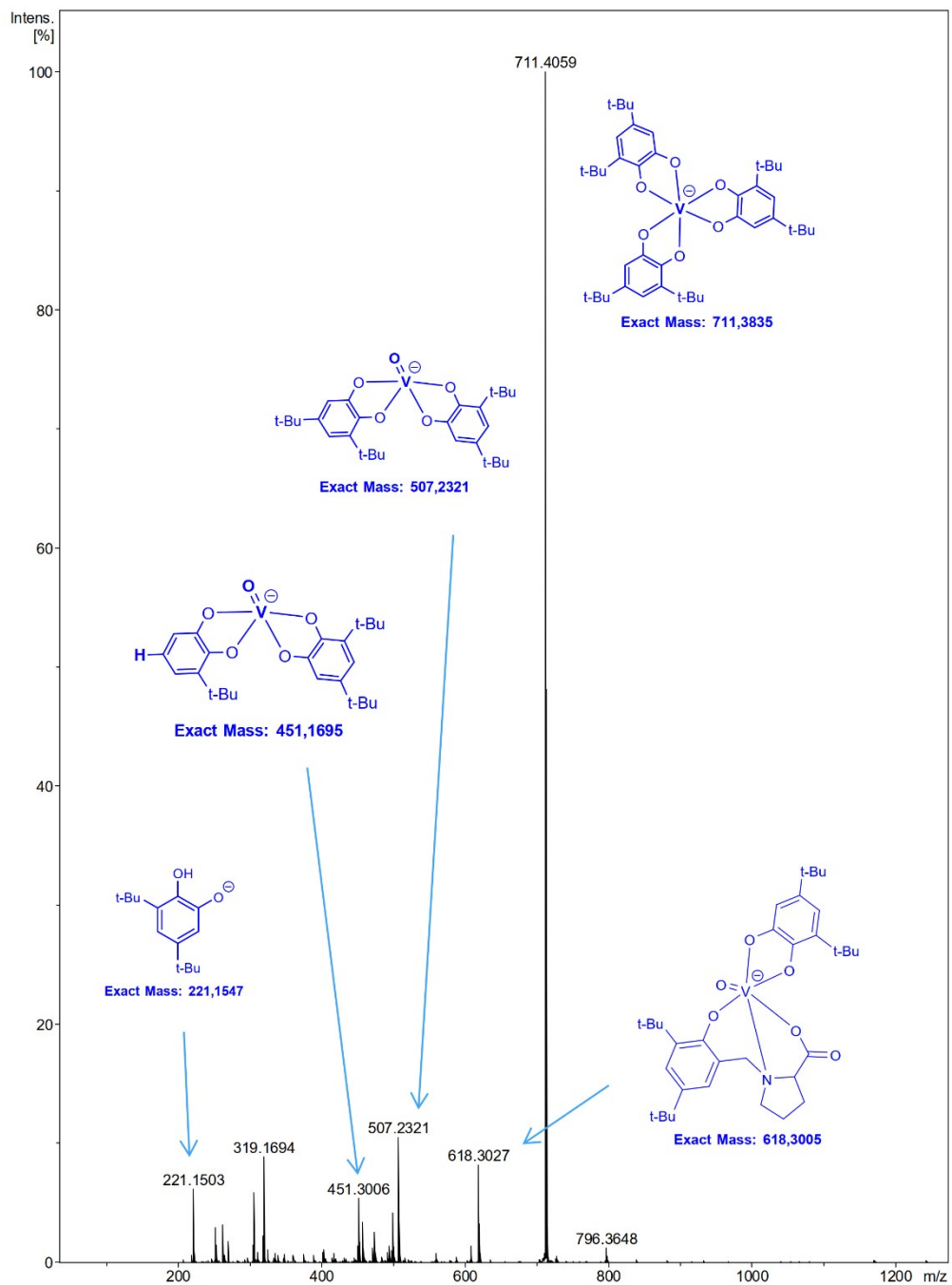


Figure S 21. Negative mode post-reaction ESI-MS spectrum of **V2** + 100 eq. 3,5-DTBC at reaction $t = 48$ h.

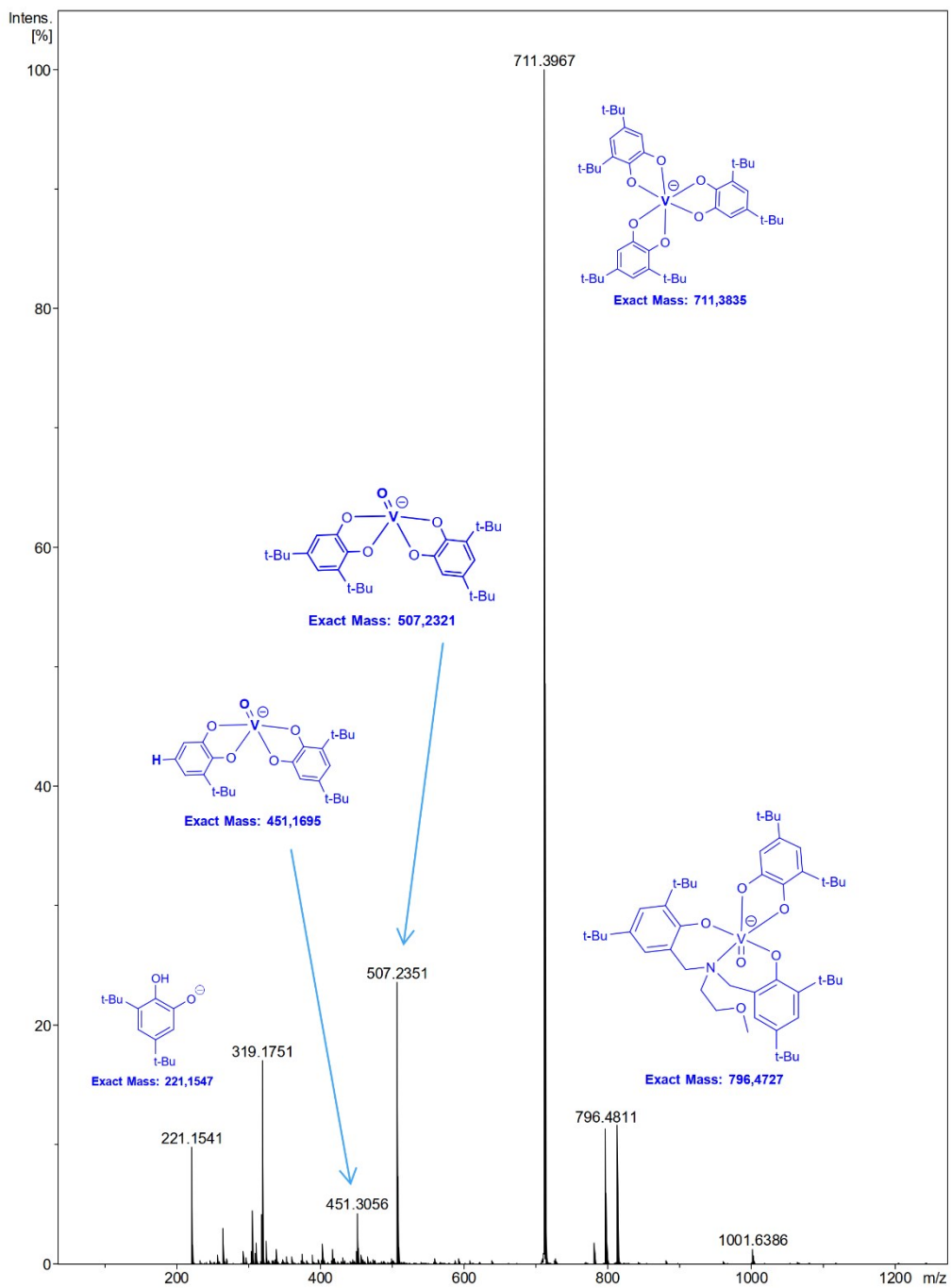


Figure S 22. Negative mode ESI-MS spectrum of **V3** + 100 eq. 3,5-DTBC at reaction $t = 30$ min.

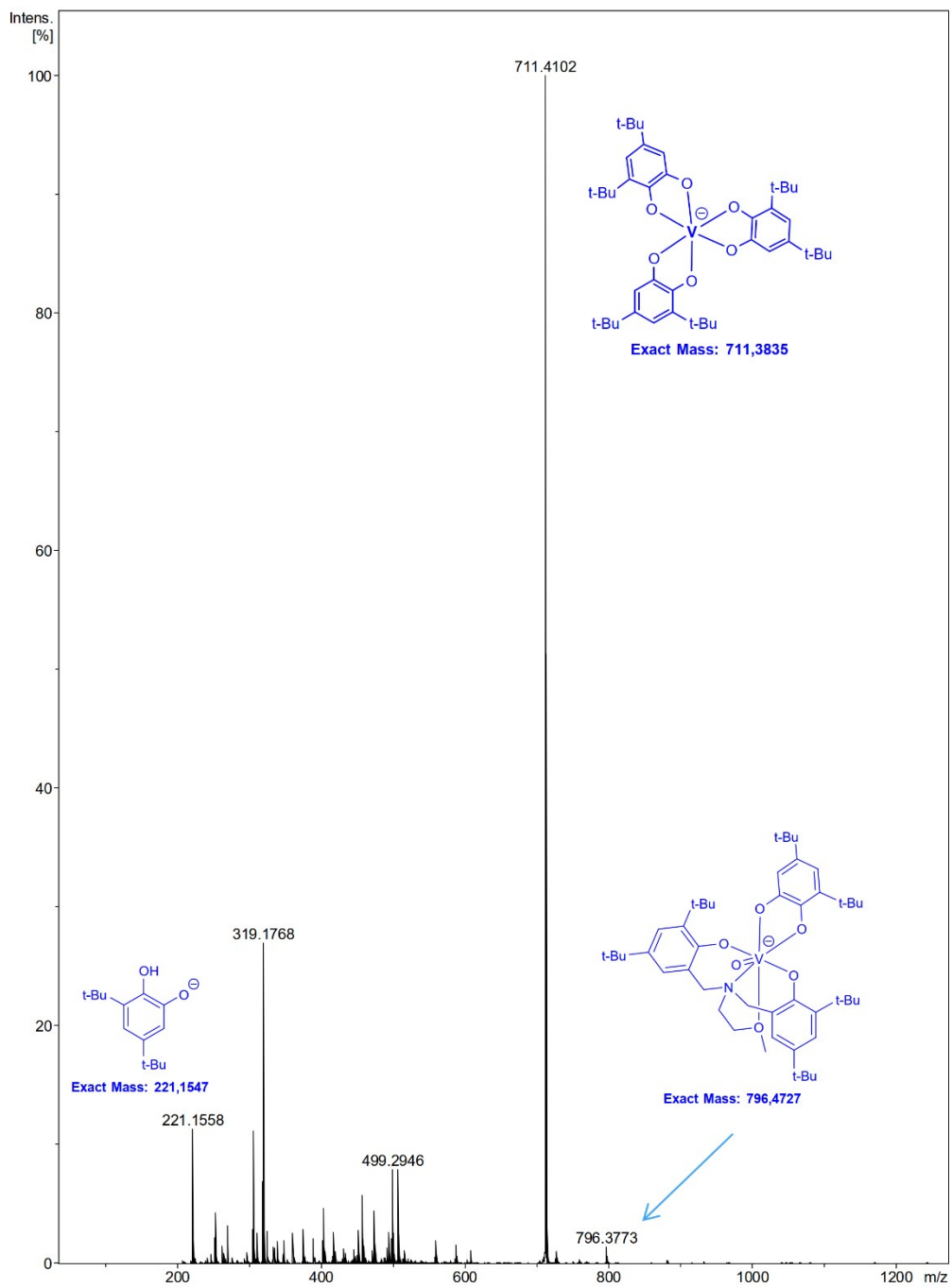


Figure S 23. Negative mode post-reaction ESI-MS spectrum of **V3** + 100 eq. 3,5-DTBC at reaction t = 48 h.

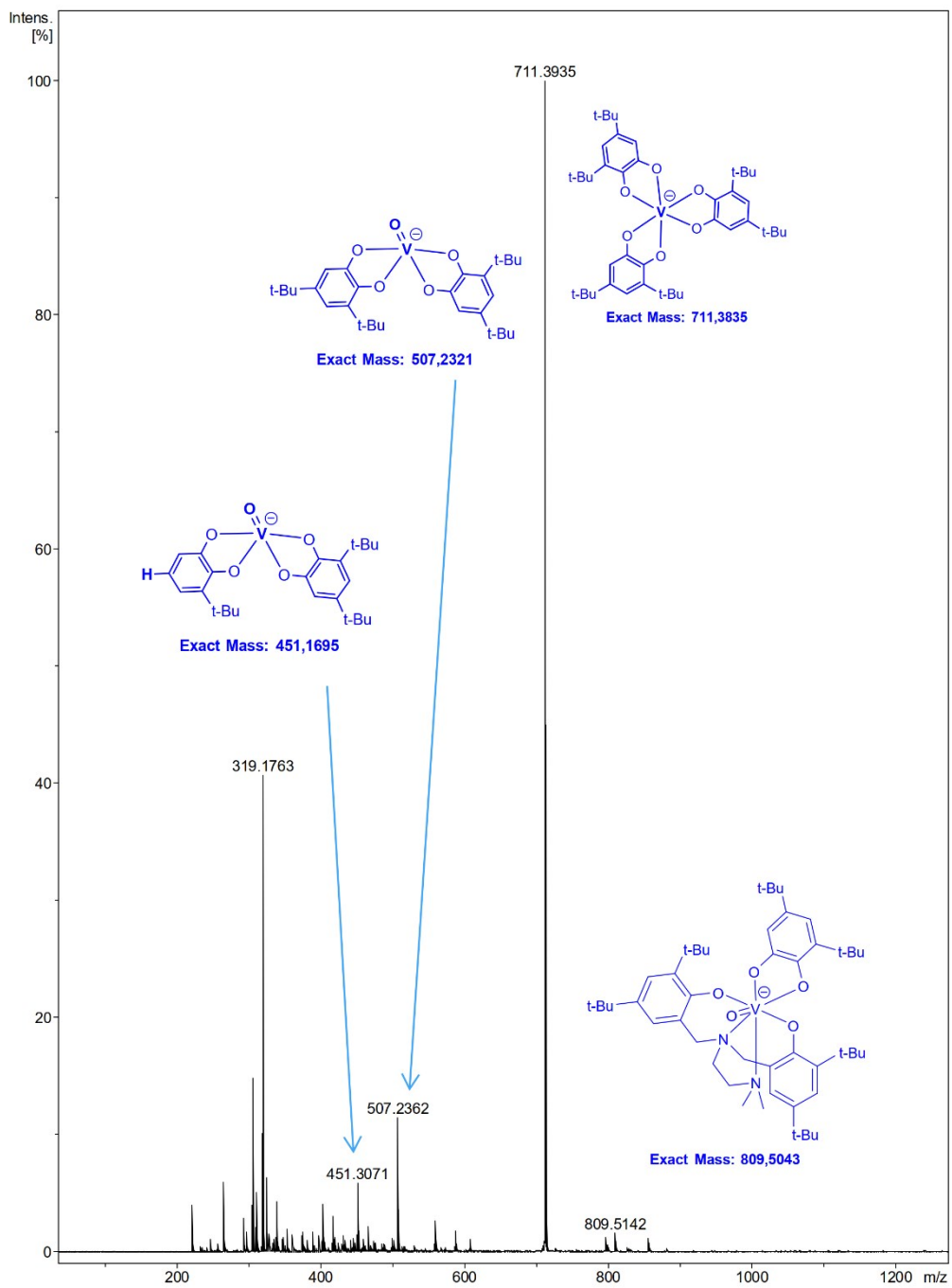


Figure S 24. Negative mode ESI-MS spectrum of **V4** + 100 eq. 3,5-DTBC at reaction $t = 30$ min.

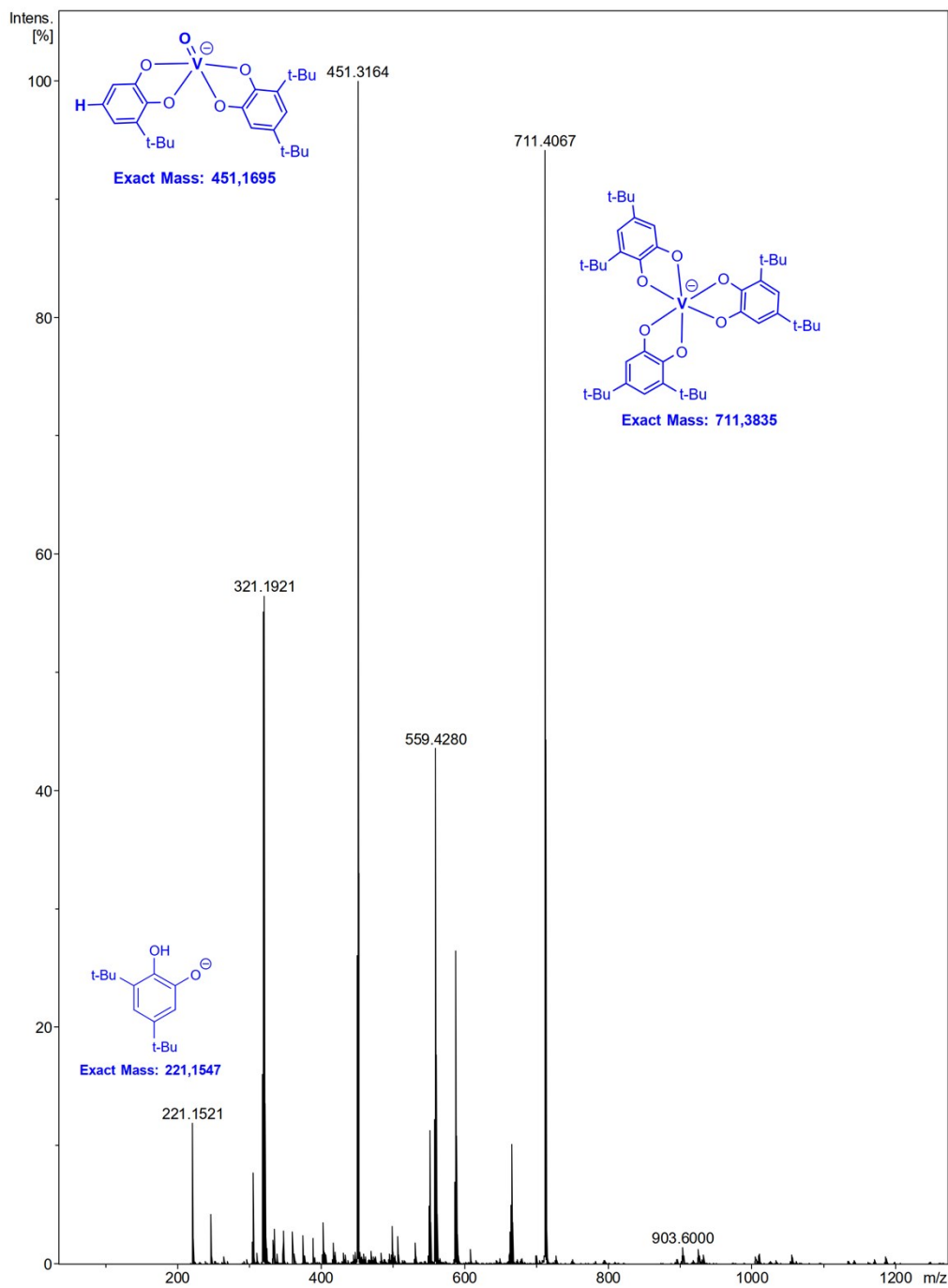


Figure S 25. Negative mode post-reaction ESI-MS spectrum of **V4** + 100 eq. 3,5-DTBC at reaction t = 48 h.

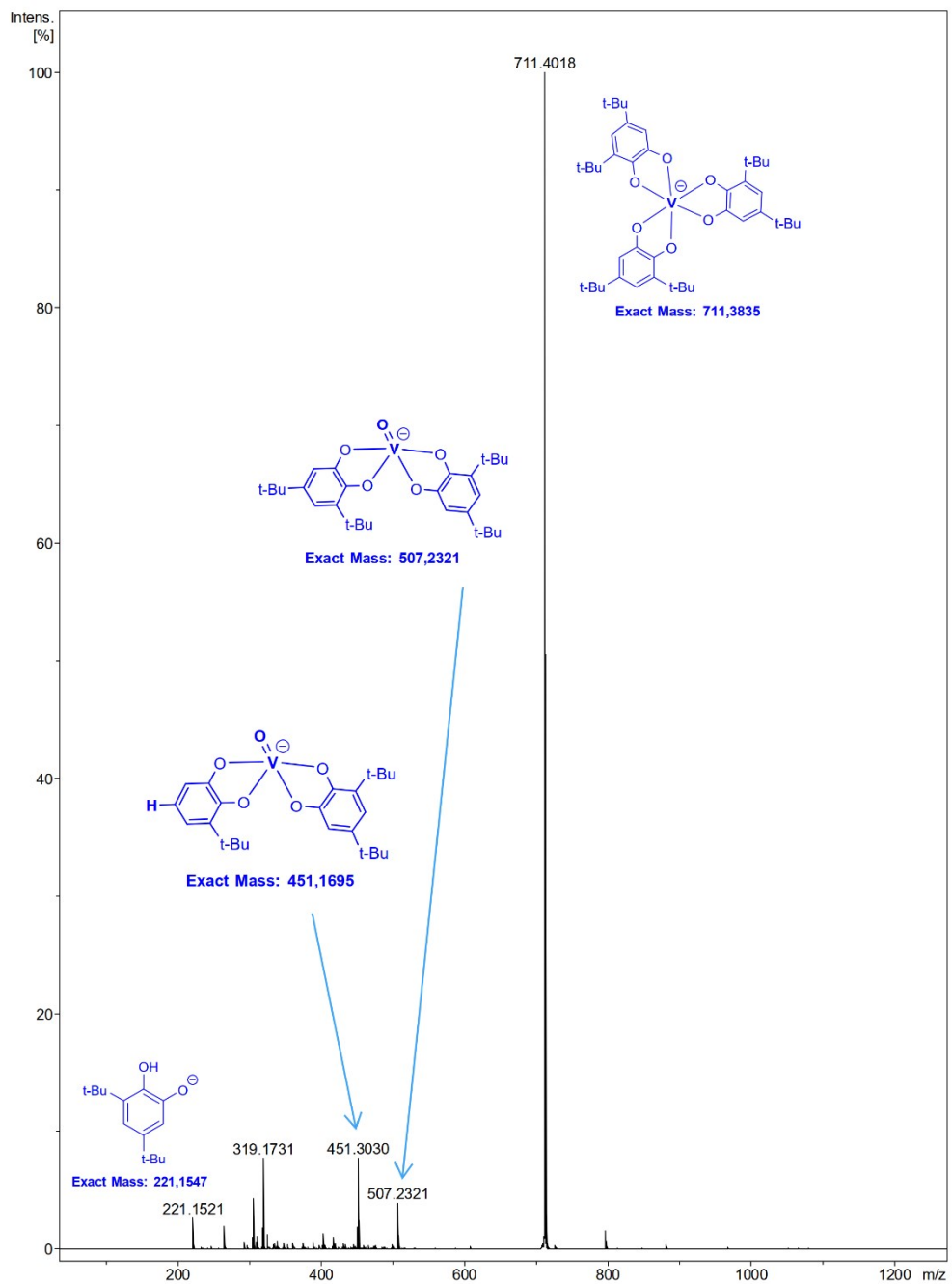


Figure S 26. Negative mode ESI-MS spectrum of **V5** + 100 eq. 3,5-DTBC at reaction $t = 30$ min.

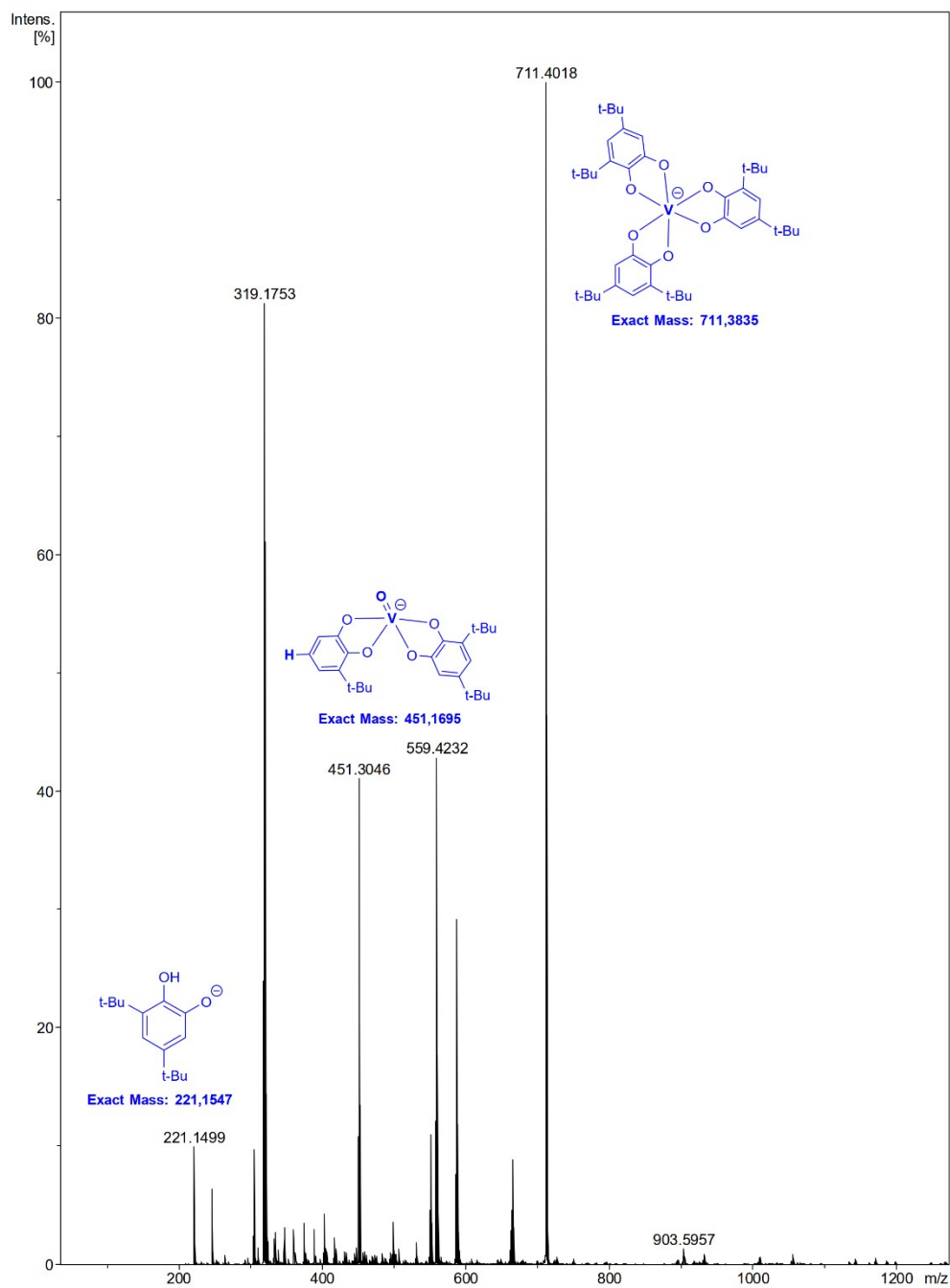


Figure S 27. Negative mode post-reaction ESI-MS spectrum of **V5** + 100 eq. 3,5-DTBC at reaction t = 48 h.

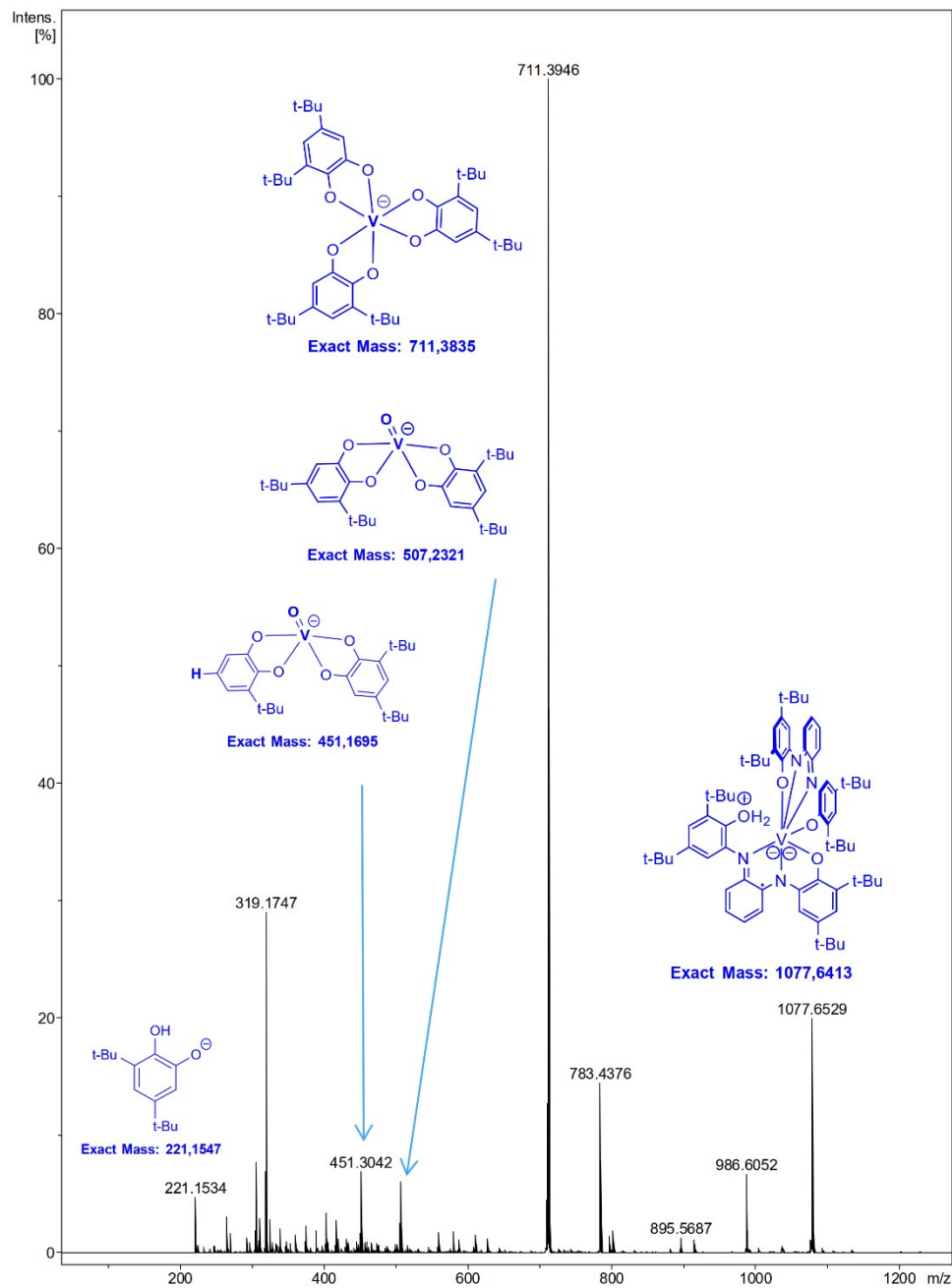


Figure S 28. Negative mode ESI-MS spectrum of **V6** + 100 eq. 3,5-DTBC at reaction $t = 30$ min.

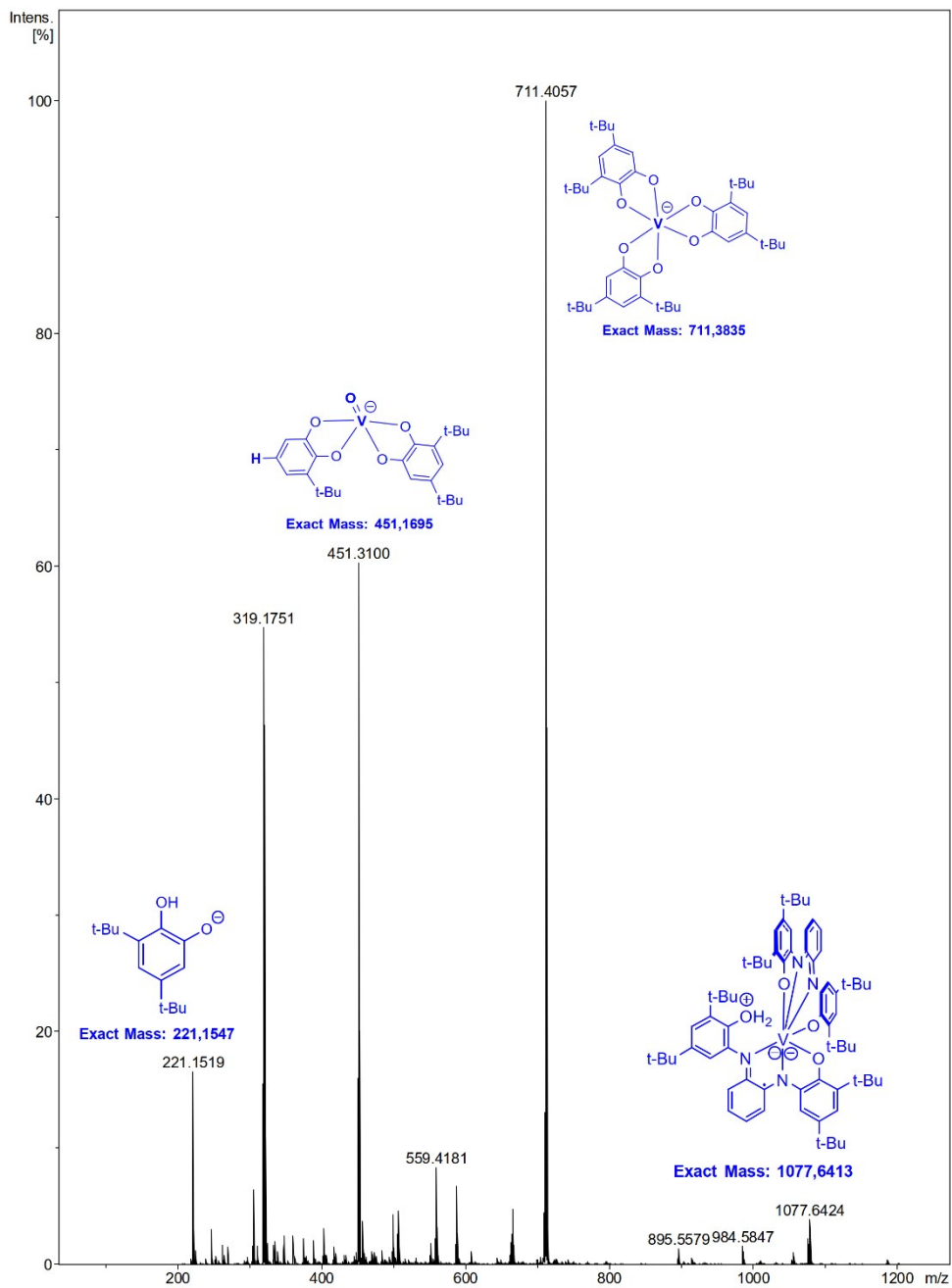


Figure S 29. Negative mode post-reaction ESI-MS spectrum of **V6** + 100 eq. 3,5-DTBC at reaction t = 48 h.

259 EPR spectroscopy

260 Discussion

261 **30 min (Figure S 30a-f):** EPR spectra recorded shortly (30 min) after treatment of **V1–V6** with 100 eq. 3,5-
262 DTBC reveal that, with the exception of **V2** (figure 30b), all complexes (figure 30a, c-f) show a rather similar
263 EPR spectrum consisting of a single absorption. With a g factor close to 2.0023 this signal most probably
264 arises from free 3,5-di-tert-butyl-1,2-semiquinone radicals. In contrast, **V2** shows a more complicated 10-
265 line EPR spectrum with a g factor of 2.0036 and a ^{51}V hyperfine coupling constant of ca. 2.05 G. This
266 spectrum is almost identical to a 10-line EPR spectrum reported for $[\text{V}(\text{3,5-DTBC})_2(\text{3,5-DTBSQ}^*)]$ with a
267 $A(^{51}\text{V}) = 2.1$ G and g factor = 2.004.[2] Given that **V2** is based on a tridentate dianionic ligand (L2, see Figure
268 S 1), instead of tetradentate dianionic ligands as is the case with **V1** and **V3–V6** it is reasonable thus to
269 conclude that **V2** has more rapidly undergone transformation compared to **V1** and **V3–6** due to
270 comparatively more facile dissociation of L2, and the more susceptible nature of **V2** towards leaching.

271 **6 hours (Figure S 31a–f):** EPR spectra recorded 6 hours after treatment of **V1–V6** with 100 eq. 3,5-DTBC
272 show little change in the case of **V2** (Figure S 31b), which still shows the characteristic signal for $[\text{V}(\text{3,5-}$
273 $\text{DTBC})_2(\text{3,5-DTBSQ}^*)]$. In the case of **V1**, **V3** and **V6** the EPR spectra show at least two signals, namely those
274 from free 3,5-DTBSQ * and $[\text{V}(\text{3,5-DTBC})_2(\text{3,5-DTBSQ}^*)]$ (Figure S 31a c and f). These findings further
275 support the notion that **V1**, **V3–V6**, bearing tetradentate ligands, degrade more slowly than **V2** to $[\text{V}(\text{3,5-}$
276 $\text{DTBC})_2(\text{3,5-DTBSQ}^*)]$, from which the active catalyst is formed by oxidation. Complexes **V4** and **V5** still
277 show a characteristic signal from a $S = \frac{1}{2}$ radical, 3,5-DTBSQ * (Figure S 31d and e).

278 **24 hours (Figure S 32a–f):** EPR spectra recorded 24 hours after treatment of **V1–V6** with 100 eq. 3,5-DTBC
279 begin to show significant changes when compared to the 6 h and 30 min spectra, respectively. For
280 example, **V1** shows an 11-line EPR spectrum (Figure S 32a) with g factor ~ 2.0034 and $A(^{51}\text{V}) \sim 2.95$ G, very
281 close to the values reported for Pierpont's complex ($g \sim 2.004\text{--}2.006$, $A(^{51}\text{V}) = 3.05$ G).[2] The 11-line
282 spectrum may suggest that $[\text{V}(\text{3,5-DTBC})_2(\text{3,5-DTBSQ}^*)]$, which gives a 10-line spectrum, might also be
283 present in some proportion. Complexes **V3** and **V5** both afford a 10-line EPR spectrum (Figure S 32c and
284 e) with g factors 2.0036 and 2.0037, and ^{51}V hyperfine coupling constants of 2.09 and 2.07 G, respectively.
285 Both agree well with the 10-line EPR spectrum reported for $[\text{V}(\text{3,5-DTBC})_2(\text{3,5-DTBSQ}^*)]$ with a $A(^{51}\text{V}) = 2.1$
286 G and g factor = 2.004.[2] The EPR spectrum of **V6**, on the other hand, is poorly resolved, but is beginning
287 to show changes towards the formation of $[\text{V}(\text{3,5-DTBC})_2(\text{3,5-DTBSQ}^*)]$ (Figure S 32f). **V2** affords the most
288 interesting EPR spectrum, clearly showing at least two distinct EPR signals (Figure S 32b). Namely, a 10-
289 line spectrum having a $g \sim 2.0035$ and $A(^{51}\text{V}) = 2.05$ G consistent with $[\text{V}(\text{3,5-DTBC})_2(\text{3,5-DTBSQ}^*)]$ is
290 observed at the center field. Additionally, an 8-line EPR signal with $g \sim 2.0021$ and $A(^{51}\text{V}) = 8.91$ G is visible
291 in the background. While the 8-line spectrum is typical for $S = 7/2$ vanadium containing complexes, the g
292 factor strongly suggests an organic radical.

293 **72 hours (Figure S 33a–f):** EPR spectra recorded 72 hours after treatment of **V1–V6** with 100 eq. 3,5-DTBC
294 start to show signs of considerable deterioration. This is expected, since Pierpont's complex is known to
295 be oxygen sensitive, slowly deteriorating to V_2O_5 and free 3,5-DTBQ.[2,3] The 72-hour measurements
296 signify the end of the EPR reaction monitoring experiments.

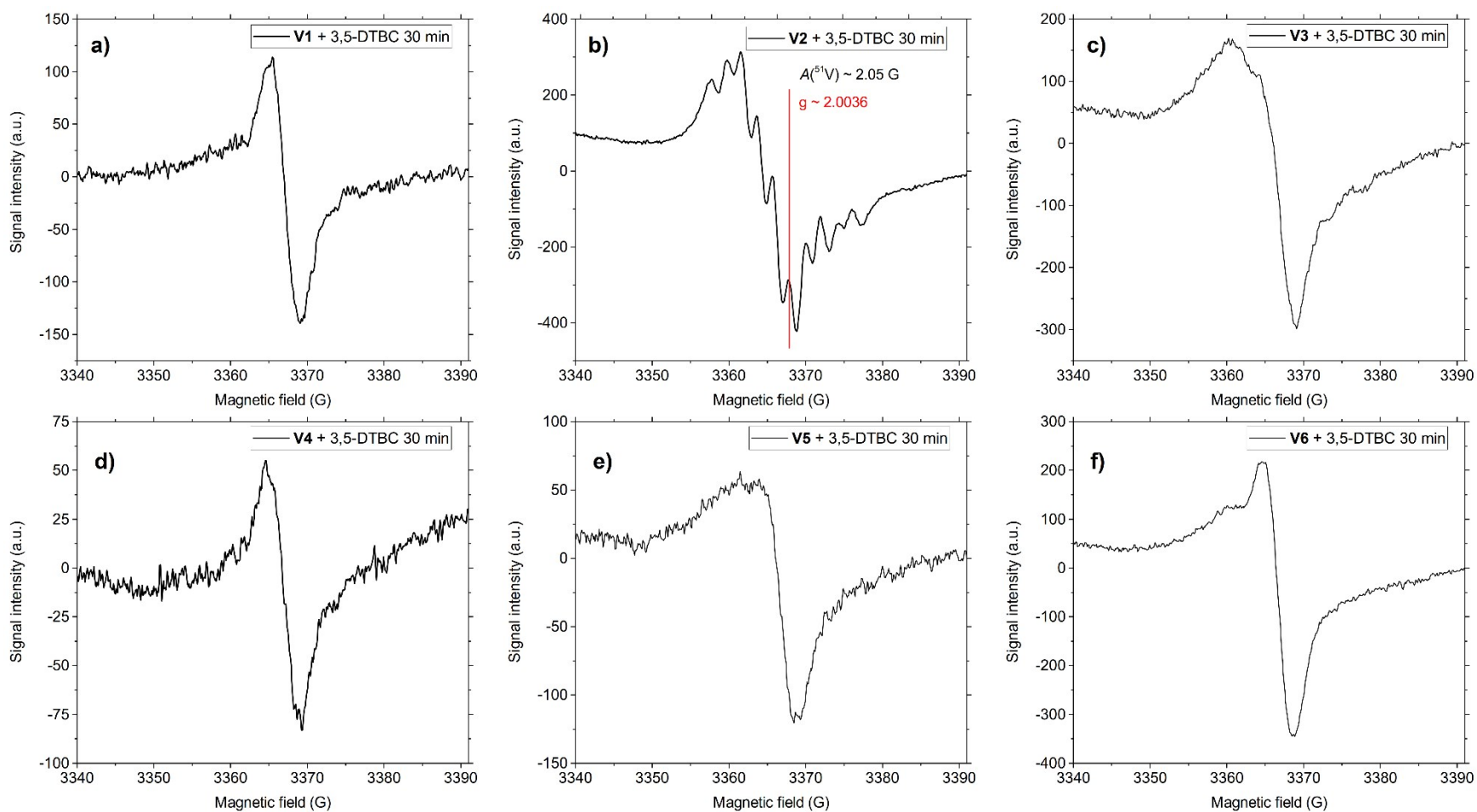


Figure S 30. Ambient atmosphere center field EPR spectra of **V1–V6** in toluene recorded at RT 30 min after treatment with 100 eq. 3,5-DTBC.

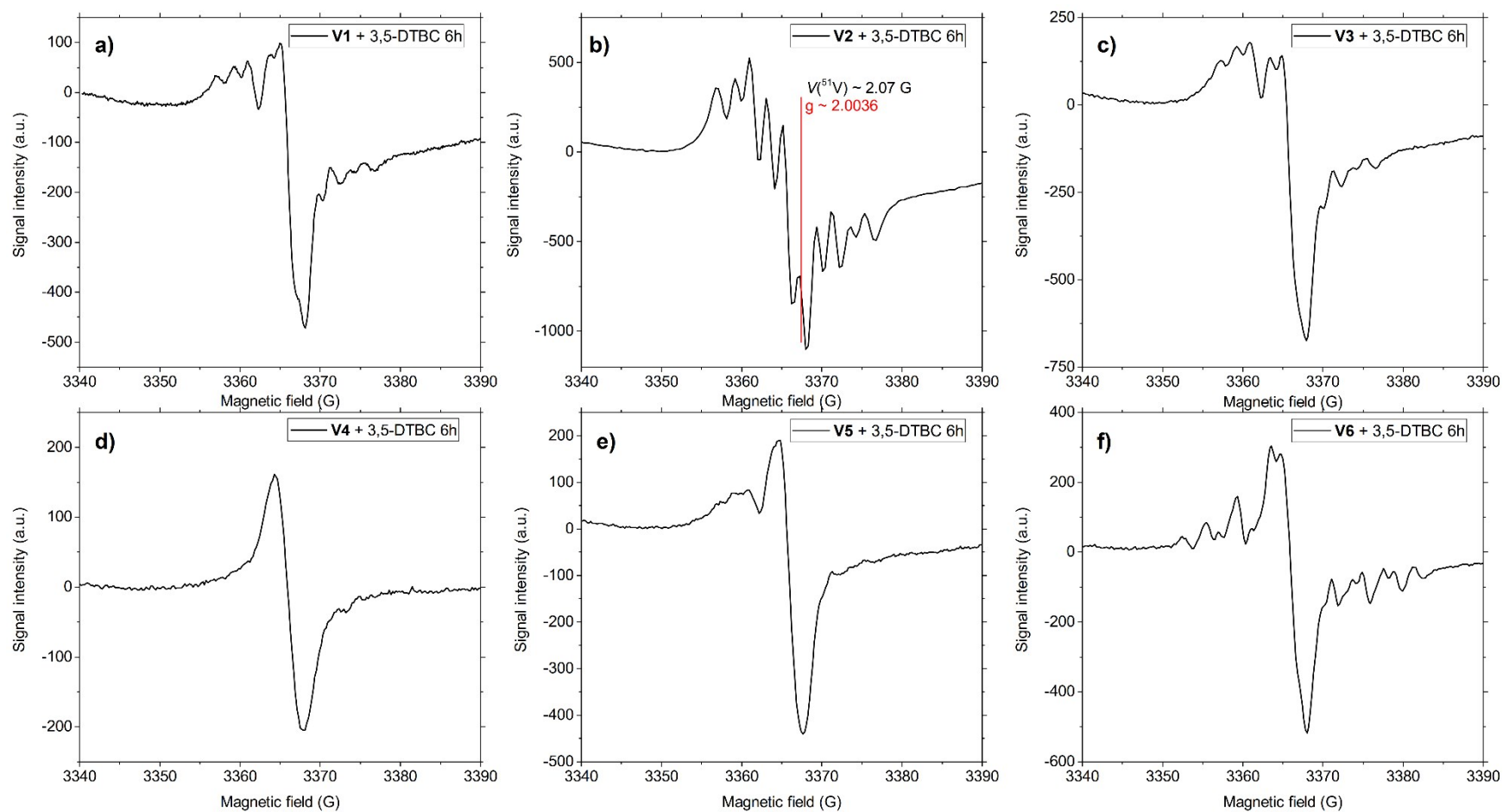


Figure S 31. Ambient atmosphere center field EPR spectra of **V1–V6** in toluene recorded at RT 6 hours after treatment with 100 eq. 3,5-DTBC.

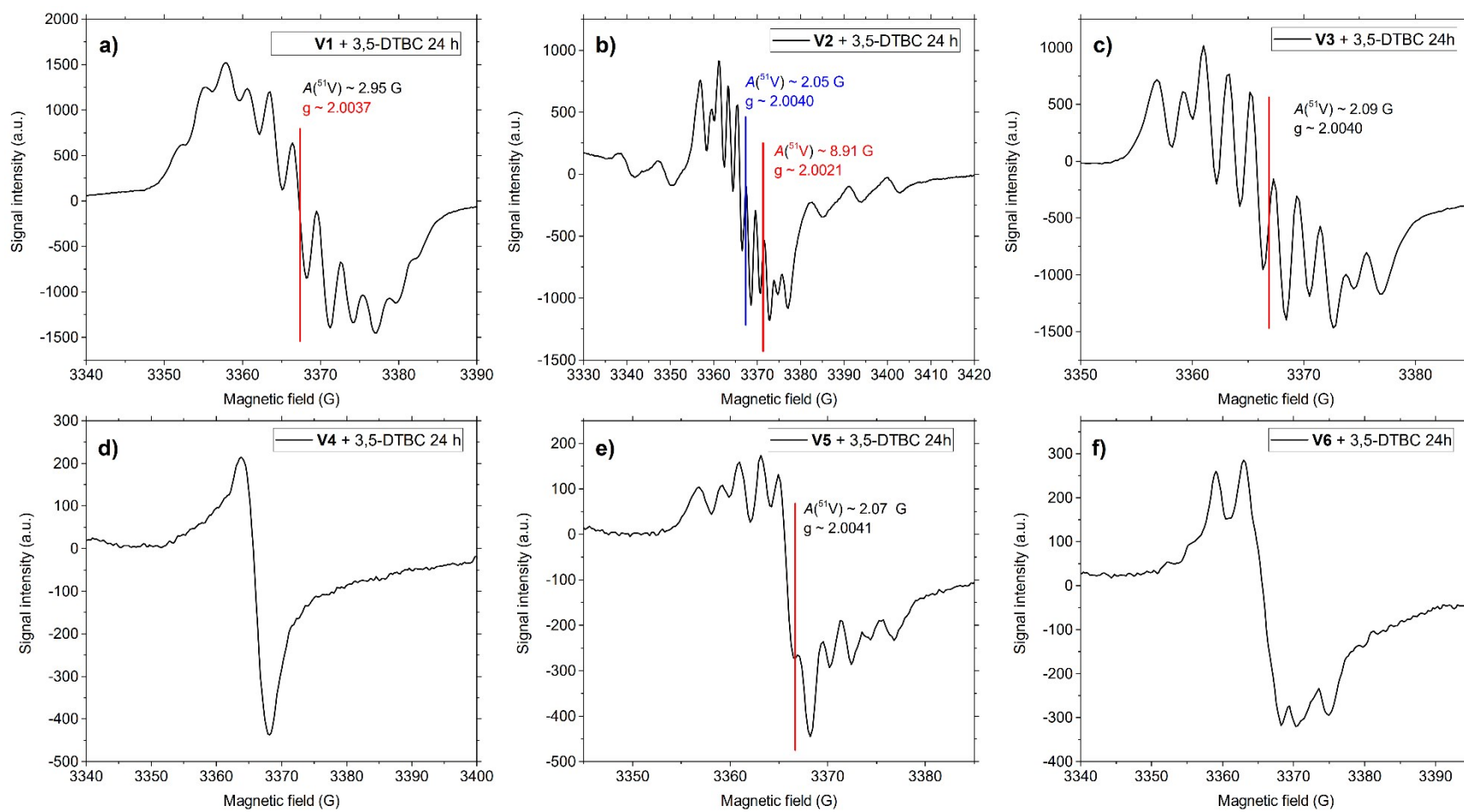


Figure S 32. Ambient atmosphere center field EPR spectra of **V1–V6** in toluene recorded at RT 24 hours after treatment with 100 eq. 3,5-DTBC.

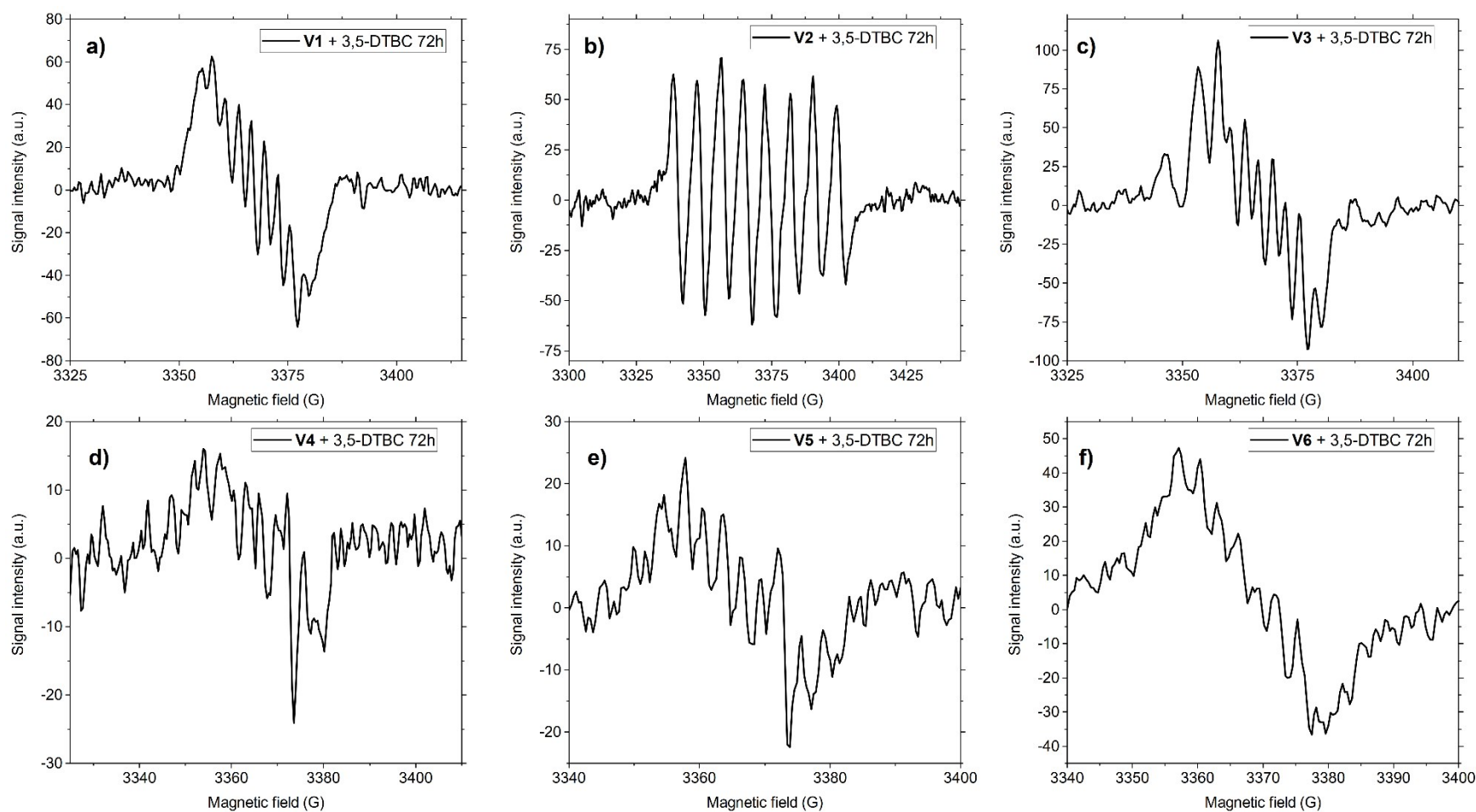


Figure S 33. Ambient atmosphere center field EPR spectra of **V1–V6** in toluene recorded at RT 72 hours after treatment with 100 eq. 3,5-DTBC.

Identification of complex giving 8-line EPR spectrum

The oxidation of 3,5-DTBC in the presence of **V2** affords an 8-line EPR spectrum with a $g \sim 2.0021 - 2.0023$ and $A(^{51}\text{V}) \sim 8.60 - 8.91$ G after 24 hours of reaction onset. At approx. 48 hours, this signal reaches its peak intensity (see figure 4b in the main text). This EPR signal is markedly different when compared to the EPR signals afforded by the other pre-catalysts at $t = 48$ hours, which all give a characteristic 9-line signal for the Pierpont's complex.

As such, attempts were made to identify this compound by EPR spectroscopy and ESI-MS spectrometry. For this purpose, ca. 1 mg of **V2** and about 44.5 mg 3,5-DTBC ($\sim 1:100$ [V]:[3,5-DTBC]) were dissolved in ca. 1 mL toluene in a test tube, and left to stand at RT in a fume hood under ambient atmospheric conditions. After ca. 48 hours of reaction onset, the characteristic 8-line EPR spectrum was once again

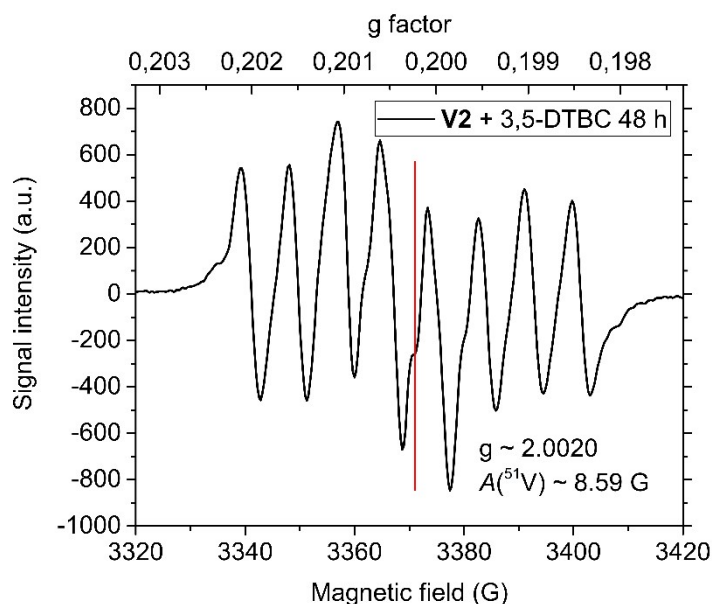


Figure S 34. Newly recorded ambient atmosphere center field EPR spectrum of **V2** in toluene at RT 48 hours after treatment with 100 eq. 3,5-DTBC.

observed (Figure S 34).

Once the 8-line spectrum was observed, the reaction mixture was sampled for negative mode ESI-MS (mass experiments performed in MeCN). The ESI-MS spectrum from this experiment (Figure S 35) reveals that species such as $[\text{V}(\text{3,5-DTBC})_2(\text{3,5-DTBSQ}^*)]$, with a $m/z = 711.3835$ (e.g. $[\text{V}(\text{3,5-DTBC})_3]^-$), and half-fragment of $[\text{VO}(\text{3,5-DTBC})(\text{3,5-DTBSQ}^*)]_2$, with $m/z = 507.2321$ (e.g. $[\text{VO}(\text{3,5-DTBC})_2]^-$), both of which are EPR active and give 10-line and 9-line spectra, respectively, are present only in very low intensity. In fact, the most intensive signal is given by $[\text{VO}(\text{L2})(\text{3,5-DTBSQ}^*)]$, with an exact $m/z = 618.3005$ (e.g. $[\text{VO}(\text{L2})(\text{3,5-DTBC})]^-$), with a found $m/z = 618.2806$. These EPR and ESI-MS experiments provide compelling, albeit perhaps not perfectly irrefutable, evidence that the 8-line EPR spectrum is in fact from $[\text{VO}(\text{L2})(\text{3,5-DTBSQ}^*)]$, which is a major component of the post-reaction medium when **V2** is used as the pre-catalyst. While we realize that a standalone synthesis and isolation of $[\text{VO}(\text{L2})(\text{3,5-DTBSQ}^*)]$ and its EPR

characterization would provide a certain answer, we did not attempt these. It should be noted, that 8-line EPR spectra with similar g and $A(^{51}\text{V})$ values have been reported for $[\text{V}(\text{TCSQ}^{\bullet})_3]$, where TCSQ^{\bullet} = tetrachloro-1,2-semiquinone.[4]

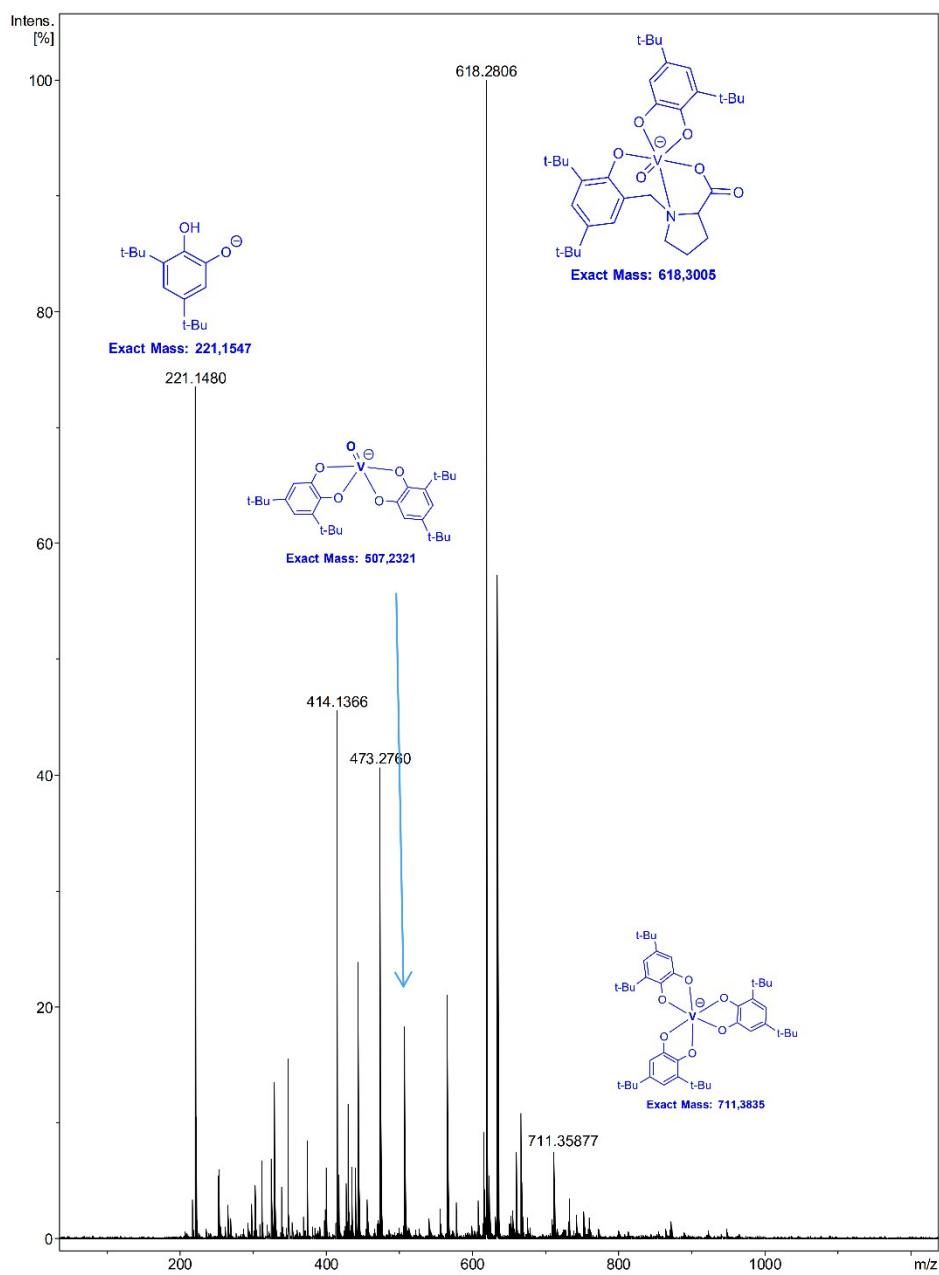
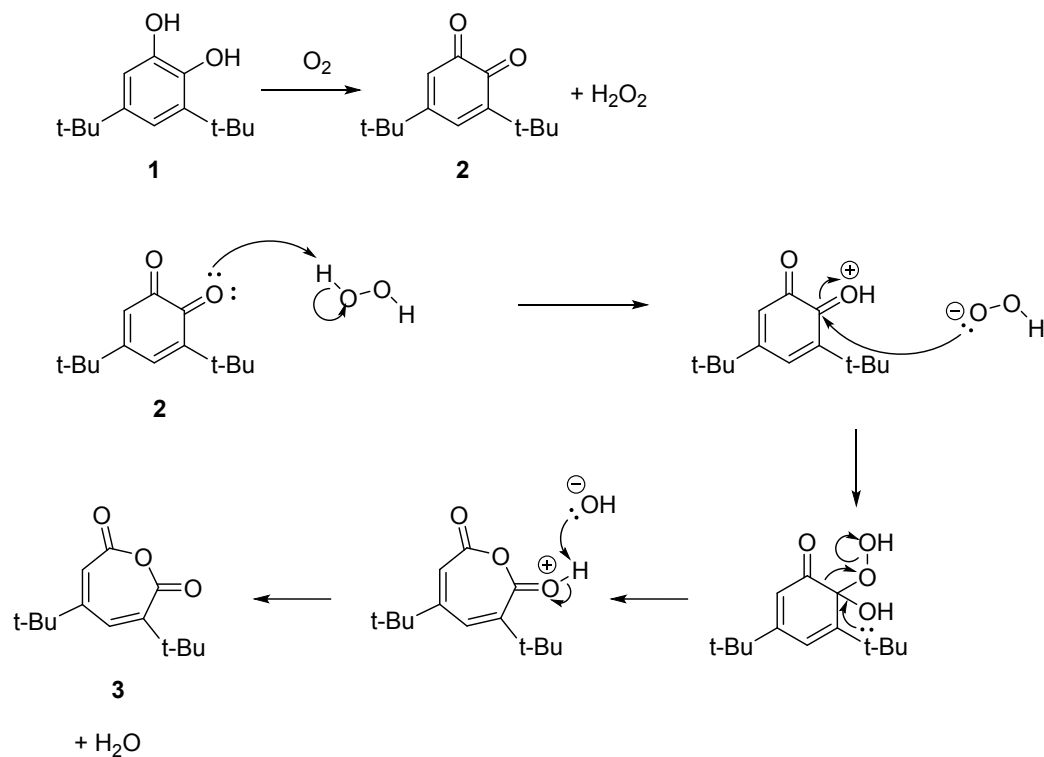


Figure S 35. Negative mode ESI-MS spectrum of **V2** at 48 hours after treatment with 100 eq. 3,5-DTBC.

Non-catalytic oxidation of 2 to 3



Scheme S 2. Facile initial O₂-mediated autoxidation of **1** to **2** as well as a proposed non-catalytic reaction mechanism involving H₂O₂-mediated Baeyer-Villiger like oxidation of **2** to the anhydride **3**. The acceleration of this reaction by Lewis acids (e.g. V⁵⁺) may be reasonably expected (see text below).

The substrate **1** is oxidized, albeit slowly, to the corresponding quinone **2** by O₂, even without catalysis. This reaction is greatly accelerated by the introduction of an organic base, such as Et₃N. The deprotonation of **1** may facilitate the oxidative formation of 3,5-di-*tert*-butylsemiquinone, which then undergoes further oxidation to **2**. In this work, the oxidation of **1** to **2** was revealed to be effected by H₂O₂, in addition to O₂. This reaction was found to be rather slow, but it may be greatly accelerated by the introduction of 1 mol-% **V1** (full conv. in 48 h), although moderate conversion (ca. 55 %) was observed without added **V1** in 48 h. The anhydride product **3** formed as a minor (yield 1–6 %) by-product in H₂O₂-mediated oxidation of **1** under *anaerobic* conditions, the higher yield obtained in the presence of **V1** and lower without a catalyst. This suggests that **3** may be formed in multiple separate ways: Firstly, **3** is the major product with yields ranging between 30–39 % in the *aerobic* **V1–V6** catalyzed pathway. This pathway corresponds to the true dioxygenase reaction, whose mechanism, as proposed by Finke,[1] is shown in ESI Scheme S1.[5,6] It is important to emphasize that in this reaction **1** is directly converted to **3**. However, **3** is also obtained in the absence of O₂ with a yield of 1 % in the presence of two eq. H₂O₂ relative to **1**. Moreover, the yield of **3** is increased to 6 % when **V1** is used as catalyst in the presence of H₂O₂. This reactivity is reminiscent of a peracid-mediated Baeyer-Villiger -like oxidation of **2**, which has been reported earlier.[7,8] It should be noted, that peracids such as *m*-CPBA are significantly more suitable oxidants for this reaction, since **2** is oxidized to **3** practically quantitatively in 5 minutes at 0 °C,[8] *versus* 1–6 % yield in 48 hours at 65 °C, as observed by us. These correspond to the second and third pathways for the formation of **3**. Namely, **3** may be obtained from **2** by direct H₂O₂-mediated oxidation without catalysts (*i.e.* Scheme S2) or *via* a Lewis

acid (vanadium(v)) catalyzed pathway, the latter of which affords **3** in a greater yield. These reactions are separate to the true dioxygenase pathway, and most likely do not play a large role in the actual O₂ dioxygenase pathway, since H₂O₂ is formed *in-situ* – *i.e.* concomitant to the formation of **2** –, and in low amounts.

References

- [1] C.X. Yin, R.G. Finke, Kinetic and mechanistic studies of vanadium-based, extended catalytic lifetime catechol dioxygenases, *J. Am. Chem. Soc.* 127 (2005) 13988–13996. doi:10.1021/ja052998+.
- [2] M.E. Cass, D.L. Green, R.M. Buchanan, C.G. Pierpont, Orthoquinone complexes of vanadium and their reactions with molecular oxygen, *J. Am. Chem. Soc.* 105 (1983) 2680–2686. doi:10.1021/ja00347a027.
- [3] C.-X. Yin, R.G. Finke, Vanadium-Based, Extended Catalytic Lifetime Catechol Dioxygenases: Evidence for a Common Catalyst, *J. Am. Chem. Soc.* 127 (2005) 9003–9013. doi:10.1021/ja051594e.
- [4] M.E. Cass, N.R. Gordon, C.G. Pierpont, Catecholate and semiquinone complexes of vanadium. Factors that direct charge distribution in metal-quinone complexes, *Inorg. Chem.* 25 (1986) 3962–3967. doi:10.1021/ic00242a027.
- [5] H.G. Jang, D.D. Cox, L. Que, A highly reactive functional model for the catechol dioxygenases. Structure and properties of [Fe(TPA)DBC]BPh₄, *J. Am. Chem. Soc.* 113 (1991) 9200–9204. doi:10.1021/ja00024a028.
- [6] C.J. Winfield, Z. Al-Mahrizy, M. Gravestock, T.D.H. Bugg, Elucidation of the catalytic mechanisms of the non-haem iron-dependent catechol dioxygenases: synthesis of carba-analogues for hydroperoxide reaction intermediates, *J. Chem. Soc. Perkin Trans. 1.* (2000) 3277–3289. doi:10.1039/b004265j.
- [7] F.R. Hewgill, S.L. Lee, Oxidation of alkoxyphenols. Part XVIII. Further examples of epoxide formation on autoxidation of moderately hindered phenols, *J. Chem. Soc. C Org.* (1969) 2080. doi:10.1039/j39690002080.
- [8] T.R. Demmin, M.M. Rogic, Preparation of muconic acid anhydrides. Characterization of the 1-oxacyclohepta-3,5-diene-2,7-dione structure, *J. Org. Chem.* 45 (1980) 1153–1156. doi:10.1021/jo01294a047.